

BRAIN COMMUNICATIONS

Magnetic resonance imaging pattern recognition in childhood bilateral basal ganglia disorders

Shekeeb S. Mohammad,^{1,2,3} Rajeshwar Reddy Angiti,^{4,5} Andrew Biggin,³ Hugo Morales-Briceño,⁶ Robert Goetti,⁷ Belen Perez-Dueñas,⁸ Allison Gregory,⁹ Penelope Hogarth,⁹ Joanne Ng,¹⁰ Apostolos Papandreou,¹⁰ Kaustuv Bhattacharya,¹¹ Shamima Rahman,¹² Kristina Prelog,⁷ Richard I. Webster,² Evangeline Wassmer,¹³ Susan Hayflick,⁹ John Livingston,¹⁴ Manju Kurian,¹⁰ W. Kling Chong¹⁵ and Russell C. Dale^{1,2,3}; Basal Ganglia MRI Study Group*

* A complete list of Basal ganglia MRI study group members can be found in the Appendix, with further details in the Supplementary material.

Bilateral basal ganglia abnormalities on MRI are observed in a wide variety of childhood disorders. MRI pattern recognition can enable rationalization of investigations and also complement clinical and molecular findings, particularly confirming genomic findings and also enabling new gene discovery. A pattern recognition approach in children with bilateral basal ganglia abnormalities on brain MRI was undertaken in this international multicentre cohort study. Three hundred and five MRI scans belonging to 201 children with 34 different disorders were rated using a standard radiological scoring proforma. In addition, literature review on MRI patterns was undertaken in these 34 disorders and 59 additional disorders reported with bilateral basal ganglia MRI abnormalities. Cluster analysis on first MRI findings from the study cohort grouped them into four clusters: Cluster 1—T₂-weighted hyperintensities in the putamen; Cluster 2—T₂-weighted hyperintensities or increased MRI susceptibility in the globus pallidus; Cluster 3—T₂-weighted hyperintensities in the globus pallidus, brainstem and cerebellum with diffusion restriction; Cluster 4—T₁-weighted hyperintensities in the basal ganglia. The 34 diagnostic categories included in this study showed dominant clustering in one of the above four clusters. Inflammatory disorders grouped together in Cluster 1. Mitochondrial and other neurometabolic disorders were distributed across clusters 1, 2 and 3, according to lesions dominantly affecting the *striatum* (Cluster 1: glutaric aciduria type 1, propionic acidemia, 3-methylglutaconic aciduria with deafness, encephalopathy and Leigh-like syndrome and thiamine responsive basal ganglia disease associated with *SLC19A3*), pallidum (Cluster 2: methylmalonic acidemia, Kearns Sayre syndrome, pyruvate dehydrogenase complex deficiency and succinic semialdehyde dehydrogenase deficiency) or pallidum, brainstem and cerebellum (Cluster 3: vigabatrin toxicity, Krabbe disease). The Cluster 4 pattern was exemplified by distinct T₁-weighted hyperintensities in the basal ganglia and other brain regions in genetically determined hypermanganesemia due to *SLC39A14* and *SLC30A10*. Within the clusters, distinctive basal ganglia MRI patterns were noted in acquired disorders such as cerebral palsy due to hypoxic ischaemic encephalopathy in full-term babies, kernicterus and vigabatrin toxicity and in rare genetic disorders such as 3-methylglutaconic aciduria with deafness, encephalopathy and Leigh-like syndrome, thiamine responsive basal ganglia disease, pantothenate kinase-associated neurodegeneration, *TUBB4A* and hypermanganesemia. Integrated findings from the study cohort and literature review were used to propose a diagnostic algorithm to approach bilateral basal ganglia abnormalities on MRI. After integrating clinical summaries and MRI findings from the literature review, we developed a prototypic decision-making electronic tool to be tested using further cohorts and clinical practice.

Received June 5, 2020. Revised August 24, 2020. Accepted September 18, 2020. Advance Access publication October 26, 2020

© The Author(s) (2020). Published by Oxford University Press on behalf of the Guarantors of Brain.

This is an Open Access article distributed under the terms of the Creative Commons Attribution Non-Commercial License (<http://creativecommons.org/licenses/by-nc/4.0/>), which permits non-commercial re-use, distribution, and reproduction in any medium, provided the original work is properly cited. For commercial re-use, please contact journals.permissions@oup.com

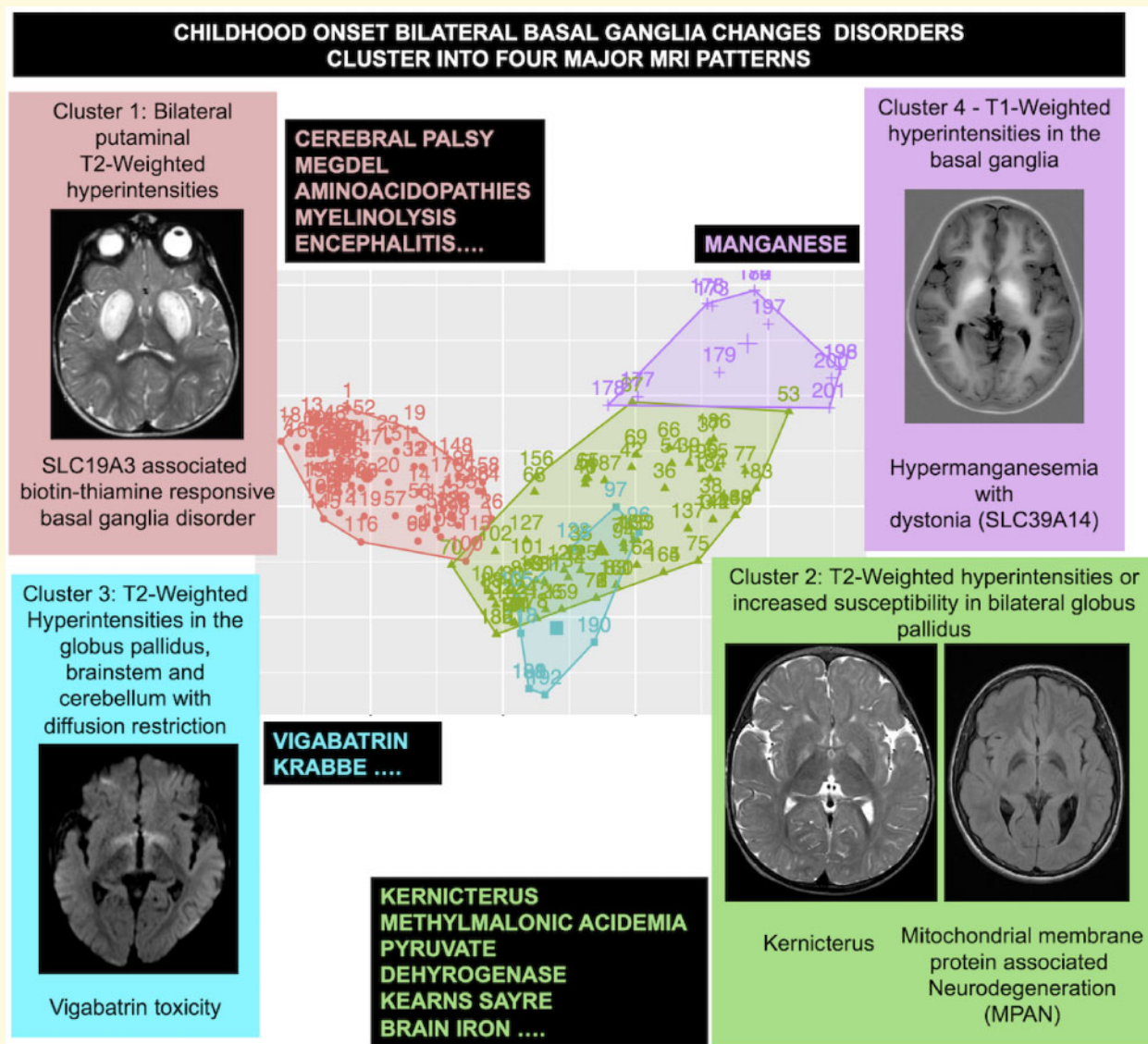
- 1 Kids Neuroscience Centre, The Children's Hospital at Westmead, Westmead, NSW 2145, Australia
- 2 TY Nelson Department of Neurology and Neurosurgery, The Children's Hospital at Westmead, Sydney, Australia
- 3 The Children's hospital at Westmead Clinical School, Faculty of Medicine, University of Sydney, Sydney, NSW 2145, Australia
- 4 Newborn and Paediatric Emergency Transport Service (NETS), Bankstown, NSW, Australia
- 5 Department of Neonatology, Liverpool Hospital, Liverpool, NSW, Australia
- 6 Movement Disorders Unit, Neurology Department, Westmead Hospital, Westmead, NSW 2145, Australia
- 7 Medical Imaging, The Children's Hospital at Westmead and Sydney Medical School, University of Sydney, Sydney, Australia
- 8 Paediatric Neurology Department, Hospital Vall d'Hebrón Universitat Autònoma de Barcelona, Vall d'Hebron Research Institute Barcelona, Barcelona, Spain
- 9 Department of Molecular and Medical Genetics, Oregon Health & Science University, Portland, OR, USA
- 10 Molecular Neurosciences, Developmental Neurosciences, UCL-Institute of Child Health, London, UK
- 11 Western Sydney Genomics Program, The Children's Hospital at Westmead and Sydney Medical School, University of Sydney, Sydney, Australia
- 12 Mitochondrial Research Group, Genetics and Genomic Medicine, Institute of Child Health, University College London and Metabolic Unit, Great Ormond Street Hospital, London, UK
- 13 Department of Paediatric Neurology, Birmingham Children's Hospital, Birmingham, UK
- 14 Department of Paediatric Neurology, Leeds Teaching Hospitals Trust, University of Leeds, UK
- 15 Department of Radiology, Great Ormond Street Hospital, London, UK

Correspondence to: Dr Shekeeb S. Mohammad, FRACP, PhD,
Clinical School, The Children's Hospital at Westmead,
Locked Bag 4001, Westmead, NSW 2145, Australia.
E-mail: shekeeb.mohammad@health.nsw.gov.au

Keywords: basal ganglia; striatum; striatal necrosis; pattern recognition; MRI

Abbreviations: ADEM = acute-disseminated encephalomyelitis; ANE = acute necrotizing encephalopathy; BG = Basal ganglia; BGE = autoimmune basal ganglia encephalitis; BPAN = beta-propeller protein-associated neurodegeneration; CP = cerebral palsy; GA1 = glutaric aciduria type 1; GP = globus pallidus; HIE = hypoxic ischaemic encephalopathy; MEGDEL = 3-methylglutaconic aciduria with deafness, encephalopathy and Leigh-like syndrome; MPAN = mitochondrial membrane protein-associated neurodegeneration; NBIA = Neurodegeneration with brain iron accumulation; PDHC = pyruvate dehydrogenase complex deficiency; PKAN = pantothenate kinase-associated neurodegeneration; PLAN = *PLA2G6*-associated degeneration; SN = substantia nigra; STN = subthalamic nucleus; T1W = T₁-weighted; T2W = T₂-weighted

Graphical Abstract



Introduction

The basal ganglia are paired deep grey matter nuclei in the brain comprised of the caudate and putamen (referred to as the 'striatum'), globus pallidus (GP), substantia nigra (SN), subthalamic nuclei (STN) and nucleus accumbens. These high energy-dependent regions of the brain are susceptible to toxic, hypoxic or ischaemic injury (Fahn, 1976; Beltz and Mullins, 2010) and have a predilection for involvement in some genetic and degenerative disorders. Progressive basal ganglia cavitation and atrophy with pathological evidence of necrosis, when involving the striatum, is termed 'striatal necrosis'. Sometimes 'striatal necrosis' is loosely and incorrectly used to lump together various basal ganglia MRI patterns (Tonduti *et al.*, 2016). A combination of clinical, biomarker and

radiological evidence is often required to reach a definite diagnosis. In presumed genetic causes, such composite evidence can help define pathogenicity of identified gene variants and assist 'reverse phenotyping' when new genetic associations are proposed. MRI, which is available worldwide, is central to this approach for disorders of the nervous system. In clinical practice, the presence of bilateral basal ganglia abnormalities has a large differential, which may prompt the use of extensive and sometimes, invasive investigations. MRI pattern recognition has been highly influential in white matter disorders, including new gene discovery (van der Knaap *et al.*, 1991; van der Knaap *et al.*, 1999; Steenweg *et al.*, 2010). Such a radiological approach for bilateral basal ganglia lesions has not been undertaken before in a cross-aetiological cohort, although narrative reviews have proposed

decision-making approaches (Ho *et al.*, 1993; Krageloh-Mann *et al.*, 2002; Finelli and DiMario, 2003; Anderson *et al.*, 2004; Lim, 2009; Hegde *et al.*, 2011; Bekiesińska-Figatowska *et al.*, 2013; Quattrocchi *et al.*, 2013; Zuccoli *et al.*, 2015; Tonduti *et al.*, 2016). In this multicentre study using a large cohort of children with MRI bilateral basal ganglia disease of broad aetiologies, we used a standard radiological scoring proforma and cluster analysis to define MRI features that group different disorders in common clusters. We further incorporated findings from literature review to develop a diagnostic algorithm and a prototypic electronic decision-making tool.

Materials and methods

Inclusion and exclusion criteria

The inclusion criteria for the study were children (0–18 years) with bilateral basal ganglia signal abnormalities reported on available MRI. We excluded cases with basal ganglia atrophy without signal abnormalities on any MRI dataset, basal ganglia hypoplasia and malformations. Disorders of neuronal migration, neoplastic disorders like neurofibromatosis, cerebrovascular insult-related basal ganglia injury and unilateral basal ganglia abnormalities were excluded as they have typical MRI appearances and do not provide the same diagnostic challenges. The first available MRI scan showing bilateral basal ganglia abnormality was included for analysis in all patients. All available subsequent scans till the age of 18 years were also evaluated. The scans were done as part of standard clinical service, hence the first included scan for some patients was not necessarily an acute scan in relation to disease onset, and timing of subsequent scans was not standardized.

Review of literature

A literature review was undertaken in Medline and EMBASE to identify conditions reported with bilateral basal ganglia MRI abnormalities. The search results include conditions described in peer-reviewed publications available in full-text format till 31 December 2019. A keyword search was done using the terms—‘MRI’ AND ‘basal ganglia, putamen, caudate, SN, subthalamic nucleus, GP, pallidum, accumbens, striatum, lentiform’, using truncation where needed. A list of possible causes of MRI basal ganglia lesions in children was drawn up to enable patient search (Supplementary Table 1).

Study cohort compilation

Patient databases—Powerchart™ at the Children’s Hospital at Westmead in Sydney, Australia and Electronic document management system™ at Great Ormond Street Hospital (GOSH) in London, UK were searched for retrospective patients with basal ganglia

changes on MRI. Ethics approval was attained at both sites (Sydney—QIE-2014-11-10, London—CA-1618/2014). The database search was undertaken using the same keywords as in the literature review as well as using individual diagnostic categories found on literature review. The database search included clinic letters, discharge summaries and MRI reports. No patients from any disease categories were excluded if they fulfilled inclusion criteria. Other experts in Barcelona, Spain, Leeds and Birmingham, UK and Portland, USA were contacted after appropriate amendment to the ethics approval and additional data transfer agreement at GOSH to contribute anonymized scans for some rare disorders identified during the literature review. All eligible scans were anonymized at export from the respective hospitals and compiled in coded DICOM folders using Horos™—a free, open source, 64-bit medical image viewer for OS X available at the time of the study under the GNU Lesser General Public License, Version 3 (LGPL-3.0) (<https://www.horosproject.org>) (June 2020, accessed). Definitions for 34 diagnostic categories for which scans were identified for this study are outlined in Supplementary Table 2.

MRI rating and proforma

The DICOM folders exported from Horos™ were reviewed and rated using SYNGO PLAZA and SYNGO FASTVIEW (© Siemens Healthcare GmbH, 2016). A scoring proforma for rating the MRI scans adapted from Pillai *et al.* (2015) was used (Supplementary Table 3). Various brain regions including each of the basal ganglia nuclei and ‘non-basal ganglia’ structures were scored for presence or absence of abnormalities on different MRI datasets. WKC, paediatric neuroradiologist at GOSH, undertook the primary rating with S.S.M., who verified the ratings before entry into the study spreadsheet. The primary raters were not blinded to the diagnosis. A random sample of 30 scans was independently rated by two paediatric neuro-radiologists R.G. and K.P. in Sydney, Australia to examine usability of the proforma. Cohen’s and Fleiss’ Kappa (for two raters) and Fleiss’ Kappa (for three raters) (Fleiss, 1971) were calculated using the online calculator available at https://www.statstodo.com/CohenKappa_Pgm.php, last accessed in June 2016. Inter-rater comparisons between K.P. and R.G. showed a mean Kappa of 0.84 (95% CI 0.67–1.00) and Inter-rater comparisons between three sets of raters (R.G., K.P., W.K.C./S.S.M.) showed a mean Kappa of 0.87 (95% CI 0.71–1.00) indicating ‘almost perfect’ agreement (Supplementary Figs 1a and b) and the rating proforma was therefore used unchanged. Where available, T₂ fluid-attenuated inversion recovery sequences were also used in scoring, but the score was coded together with the T₂ weighted (T2W) category. Susceptibility weighted sequences such as SWI/SWAN/T2* were scored as ‘increased susceptibility’ based on age and conventional departmental reporting practice. The term ‘increased susceptibility’

in the context of MRI reporting and the remainder of this paper implies hypointense signal on susceptibility-weighted sequences.

Statistical analysis

Statistical analysis was performed using SPSS v20.0.0. Proportions between the groups were compared using Chi-square test. Medians were compared using non-parametric tests—Mann-Whitney *U* test or Kruskal–Wallis.

Cluster analysis

Agglomerative hierarchical clustering analysis was performed using ‘R’ software for statistical computing (R Core Team, 2019). Twenty-three MRI features on the first included MRI scan were used for the cluster analysis. These MRI features were based on the location of MRI abnormality and type of MRI abnormality (e.g. increased susceptibility/T1W hyperintensity, etc.), derived from the main study data (Supplementary Section 1) and were scaled before entering into the clustering algorithm. Various dissimilarity measures (Euclidean, Manhattan and Minkowski) were used with different agglomeration methods (Ward, single, complete, average, weighted and gaverage). Incremental cluster plots from 2 to 8 were generated using multiple clustering methods and analysed using NbClust, an ‘R’ Package (Charrad *et al.*, 2014) which helped determine the optimal number of clusters. Each patient was represented by a unique number in the cluster plots. Cluster validation statistics showed Euclidean dissimilarity measure with average agglomeration method as the ‘best-fit’ algorithm for cluster generation (Fig. 1 and Supplementary Fig. 2). Patients in each cluster were compared using proportions and chi-square test (for presence of distinguishing MRI abnormalities that separated them into different clusters or similar MRI abnormalities that clustered them together). Discriminatory MRI features were used to generate a proportion-based heatmap (Fig. 2). Representative images were selected to highlight MRI patterns in the four clusters (Figs 3–5). MRI features differentiating the study cohort into four Euclidean-average clusters were integrated with findings from the literature review to develop a branching algorithm (Fig. 6 and Supplementary Section 2).

Development of a decision-making application

The presence or absence of 30 discrete MRI abnormalities was categorized for each of the 34 diagnostic categories from this study. MRI data from a further 59 diagnostic categories from literature review, corresponding to the same 30 MRI abnormalities were incorporated into the categorization along with clinical summaries (Supplementary Table 5). As described in Supplementary Section 3, categorization for the study cohort was modified after literature review to account for MRI changes

not noted in this study cohort but described in literature (if required). The final categorization was used to build a standalone electronic application (available for download from <http://www.kidsneuroscience.org.au/resources-epilepsy>) using FileMaker Pro 16 Advanced™ (FileMaker, Inc.). Example images were incorporated in the application for diagnostic categories included in the study and selected references for other diagnostic categories from literature review are provided in Supplementary Table 6 to direct readers to typical imaging examples. This pilot application is based on results from this study and literature review, requires validation and should not be used for clinical decision-making.

Data availability

The data that support the findings of this study are available from the corresponding author, upon reasonable request. The electronic tool described is downloadable from <http://www.kidsneuroscience.org.au/resources-epilepsy> (October 2020, accessed).

Results

Three hundred and five MRI brain scans from 201 patients were reviewed and rated. Two or more sequential scans were available for 84/201 patients. The distribution of patients across various diagnostic categories is detailed in Table 1. Forty per cent of the scans were done on a 1.5 Tesla (T) MRI machine (GE, Siemens) and the remaining on 3.0 T Machines (GE, Siemens). Clinical syndromes are used to describe most categories, but gene notations are used for recent disorders where syndromic descriptions are still expanding.

The ‘best-fit’ Euclidean-average algorithm resulted in most diagnostic categories segregating into one of four discrete clusters (Figs 1 and 2, third column) based on ratings from their first included MRI scans. Only a smaller fraction of patients (7/201) in some diagnostic categories [ADAR-1/7, mitochondrial complex 1 deficiency-2/5, Kearns Sayre syndrome-1/5, propionic acidemia-1/11, pyruvate dehydrogenase complex deficiency (PDHC)-1/6 and hypermanganesemia associated with *SLC39A14*-1/6] were represented in a second cluster, while still showing dominant clustering in one cluster. MRI abnormalities noted to contribute to clustering are represented as proportion of patients within each diagnostic category in Fig. 2.

Bilateral basal ganglia abnormalities can be segregated into four different clusters

MRI scans grouped together in one of four clusters (Fig. 1) based on the following findings from their first included scans:

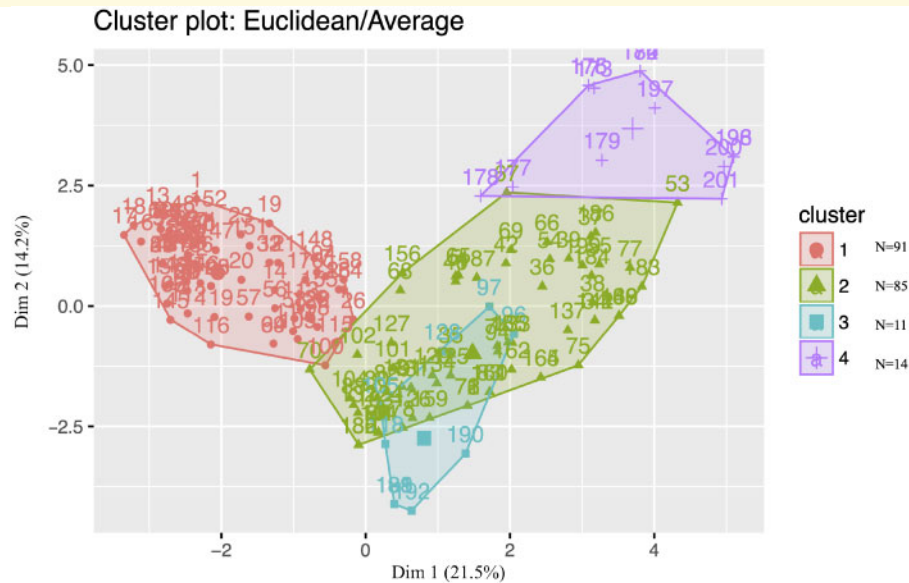


Figure 1 'Best fit' Euclidean-average four cluster plot. Cluster plot derived using Euclidean distance and average agglomeration algorithm divides the cohort of 201 first MRI scans into four clusters. Each individual number within the clusters represents one patient. The major MRI features that determined cluster distribution are: Cluster 1: T2W hyperintensities in the putamen, Cluster 2: T2W hyperintensities or increased susceptibility in the GP/SN/STN, Cluster 3: T2W hyperintensities in the GP, brainstem and cerebellum with diffusion restriction and Cluster 4: T1W hyperintensities in the basal ganglia without T2W hyperintensities or diffusion restriction. Dim, dimension; GP, globus pallidus; SN, substantia nigra; STN, subthalamic nucleus.

- Cluster 1: T2W hyperintensities in the putamen
- Cluster 2: T2W hyperintensities or increased susceptibility in the GP
- Cluster 3: T2W hyperintensities in the GP, brainstem and cerebellum with diffusion restriction
- Cluster 4: T1-weighted (T1W) hyperintensities in the basal ganglia.

Cluster 1: Bilateral putaminal T2W hyperintensities

The presence of bilateral putaminal T2W hyperintensities was the major determinant for 91/201 patients from 15 different diagnostic categories to group together in Cluster 1 (Fig. 2). In addition, Cluster 1 had a higher number of patients as a proportion of the whole cohort with T2W hyperintensities in the caudate, thalamus, white matter and cortical grey matter as well as with cortical grey matter atrophy (Fig. 3A). Conversely, very few patients in Cluster 1 demonstrated any MRI abnormalities in the GP or cerebellum. Within Cluster 1 some typical patterns of abnormalities were observed in different diagnostic categories. A distinct pattern was noted in the striatum in all patients with 3-methylglutaconic aciduria with deafness, encephalopathy and Leigh-like syndrome (MEGDEL) with spared sections in the putamen sandwiched between anterior and posterior sections of T2W hyperintensities (Fig. 3B). Partial sparing of regions within the putamen was also noted in single cases with

ADAR, mitochondrial complex 1 deficiency and *SLC19A3*. A rim-like distribution of more prominent T2W hyperintensity around the putaminal edge and sometimes including surrounding structures was noted in acute-disseminated encephalomyelitis (ADEM)(1/11), acute necrotizing encephalopathy (ANE)(3/5) (Fig. 3C), autoimmune basal ganglia encephalitis (BGE)(1/10), myelinolysis (2/3) (Fig. 3D) and *SLC19A3* (1/6). All patients with cerebral palsy due to hypoxic ischaemic encephalopathy (HIE) at term (referred hereafter as CP) had a typical pattern of T2W hyperintensities in bilateral motor strips, corticospinal tracts in the internal capsules, posterior putamina and ventrolateral thalami (Fig. 3E and F). Thalamic T2W hyperintensities with diffusion restriction were seen with swelling of the thalami in all cases of ANE (Fig. 3C), while distinct linear T2W hyperintensities were noted in the internal medullary lamina of the thalami in cases with propionic acidaemia (Fig. 3G). Prominent swelling of the putamina was noted in 38/91 patients across Cluster 1, sometimes appearing very striking, as in cases with *SLC19A3* (Fig. 3H). Cortical grey matter T2W hyperintensities were noted in a patchy distribution in ADEM, infectious encephalitis and mitochondrial complex 1 deficiency and were diffuse and homogenous in BGE, while changes with distinct patterns were noted in other diagnostic categories—external capsule (ANE), motor cortex (CP) (Fig. 3F) and a unique multifocal pattern with diffusion restriction (*SLC19A3*) (Fig. 3I). T2W hyperintensities in the white matter in

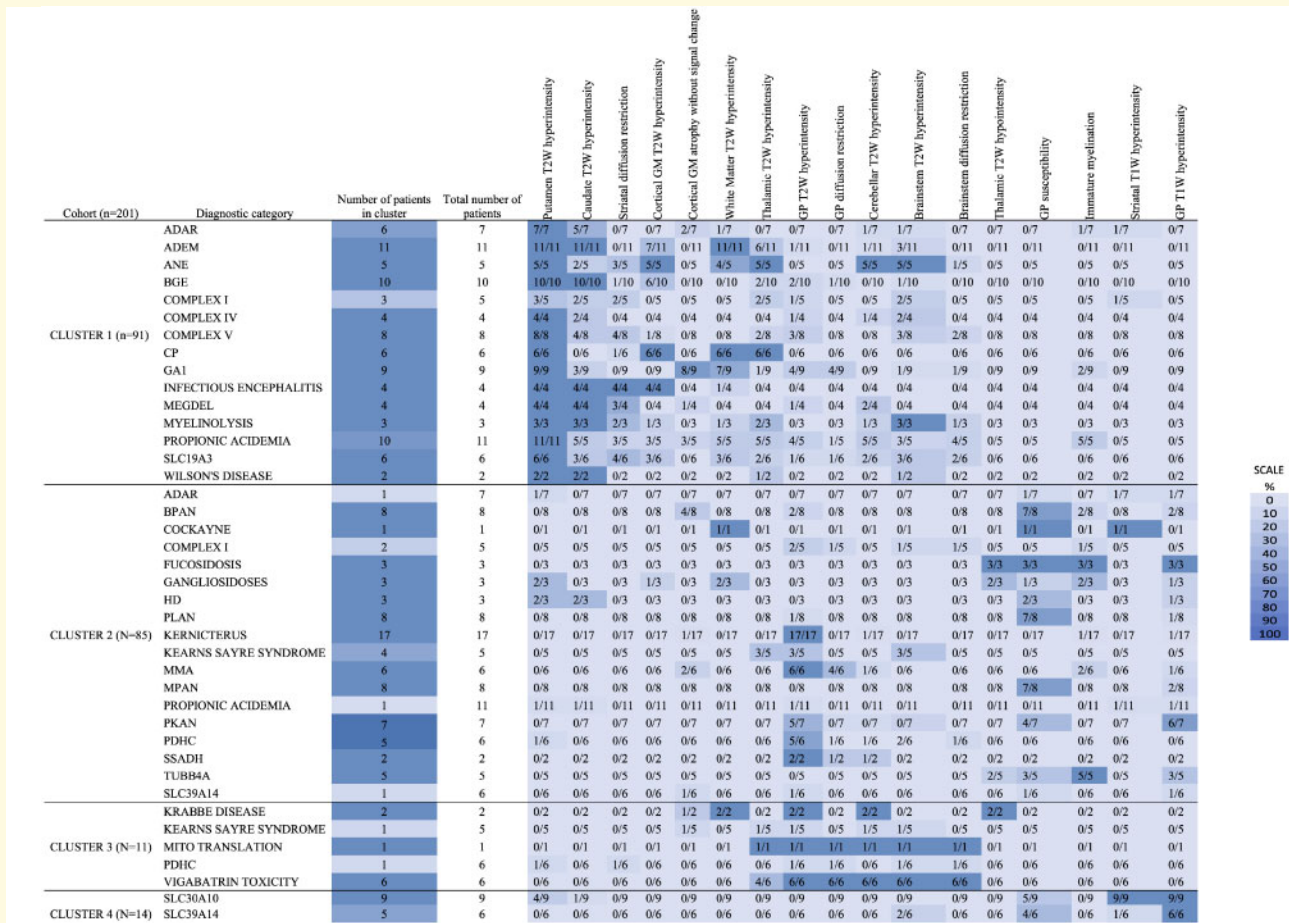


Figure 2 Proportion-based heatmap of selected MRI features on first included scan. The figure describes the presence and absence of specific MRI features on the first included MRI from 201 patients. Diagnostic categories are shown in the second column and are organized according to grouping in one of four clusters depicted in the first column. The third column shows the number of cases for each diagnostic category that grouped in the respective cluster depicted by the heat map shading as per the included scale. Increasingly darker shades depict higher proportions of patients. The fourth column shows the total number of cases for each diagnostic category included in the study. The remaining cells provide a heat map of the proportion of patients in each diagnostic category demonstrating the specific MRI features. An overall picture of the percentage of patients demonstrating specific MRI features can be gained by the heat map colour scheme with the included scale providing a guide to increasing proportion of patients with increasing depth of the blue shading. ADEM, acute-disseminated encephalomyelitis; ANE, acute necrotizing encephalopathy; BGE, autoimmune basal ganglia encephalitis; BPAN, beta-propeller protein-associated degeneration; CP, cerebral palsy; GAI, glutaric aciduria type I; GM, grey matter; GP, globus pallidus; MEGDEL, 3-methylglutaconic aciduria with sensori-neural deafness, encephalopathy, and Leigh-like syndrome; MMA, methyl malonic acidemia; MPAN, mitochondrial membrane protein-associated neurodegeneration; PDHC, pyruvate dehydrogenase complex deficiency; PKAN, panthothenate kinase-associated degeneration; PLAN, *PLA2G6*-associated neurodegeneration; SSADH, succinic semialdehyde dehydrogenase deficiency.

patients in Cluster 1 were typically multifocal in the sub-cortical white matter in ADEM, while these were dominantly seen in the parasagittal white matter and corticospinal tracts in CP and non-specific in other diagnostic categories.

In Cluster 1, 50/91 patients had one or more sequential MRI scans that were rated as a part of this study. Only 4/50 of these patients (3/11 with ADEM, 1/6 with *SLC19A3*) showed complete resolution of all MRI abnormalities in their final sequential scan. One additional patient with ADEM and 2/4 with infectious encephalitis showed resolution of basal ganglia abnormalities while still

showing MRI abnormalities in other brain regions in their final sequential scan. Striatal atrophy was noted in 27/50 patients from Cluster 1 on follow-up scans with both cystic change and atrophy in the striatum noted in 7/50 patients.

Cluster 2: T2W hyperintensities or increased susceptibility in bilateral GP

The first MRI scan of 85 patients from 18 diagnostic categories who grouped together in Cluster 2 showed either

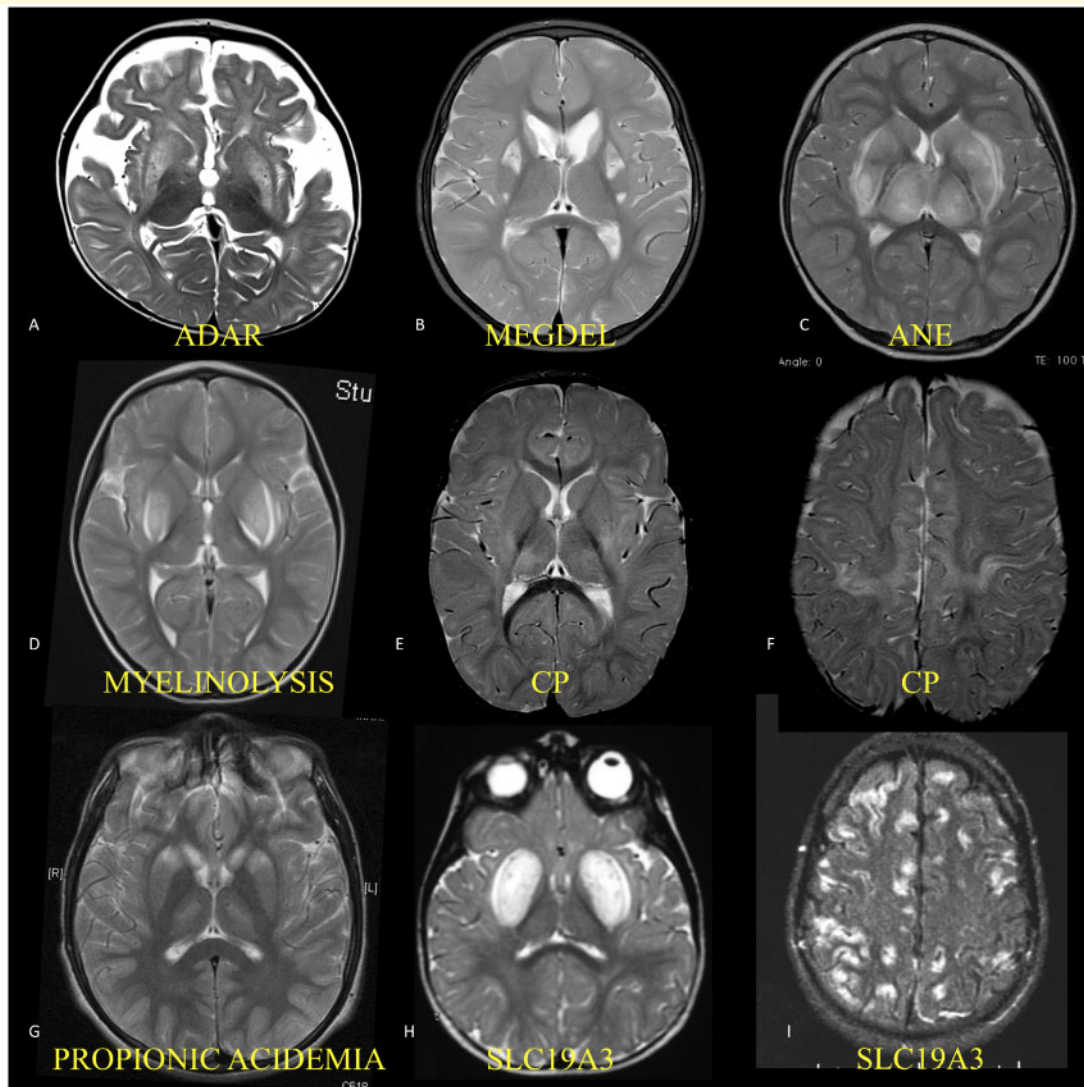


Figure 3 Cluster 1. T2W (A–H) and diffusion (I) axial MRI images from patients in Cluster 1, all of whom had putaminal T2W hyperintensities. (A) MRI of a 9-month-old boy with bi-allelic ADAR mutations showing bilateral T2W hyperintensities in the putamina along with bilateral fronto-temporal atrophy; (B) MRI of an 18-month-old girl with MEGDEL associated with bi-allelic SERAC1 mutations showing bilateral T2W hyperintensities with regions of sparing in the posterior third of both putamina; (C) MRI of a 3-year-old boy with sporadic ANE showing patchy T2W hyperintensities in bilateral putamina and thalami, thalamic swelling and a rim of T2W hyperintensity in the external capsule and claustrum around both putamina; (D) MRI of a 16-year-old girl with myelinolysis showing T2W hyperintensities in bilateral posterior putamina along with a rim of brighter T2W hyperintensities along the internal and external capsules around the putamina; (E) MRI of a 6-year-old boy with dystonic CP after HIE at birth (40 weeks of gestation) showing T2W hyperintensities in posterior putamina and ventrolateral thalami; (F) MRI of the same 6-year-old boy as in 'E' with dystonic CP showing T2W hyperintensities in the cortical grey matter in bilateral rolandic regions and parasagittal regions as well as surrounding white matter; (G) MRI of a 4-year-old girl with propionic acidemia showing T2W hyperintensities in bilateral caudate nuclei and anterior putamina along with linear T2W hyperintensities in the internal medullary lamina of bilateral thalami; (H) MRI of a 3-year-old boy with thiamine responsive basal ganglia disease associated with bi-allelic SLC19A3 mutations at presentation showing bilateral putaminal swelling and T2W hyperintensity; (I) MRI of a 2-year-old girl with thiamine responsive basal ganglia disease associated with bi-allelic SLC19A3 mutations at presentation showing bilateral, extensive multifocal regions of cortical grey matter diffusion restriction.

T2W hyperintensities or increased susceptibility in bilateral GP (Fig. 2). In addition, most patients with immature myelination and cerebellar atrophy grouped together in Cluster 2. Bilateral T2W hypointensities of the ventrolateral thalami were noted in 7/85 patients in Cluster 2. The thalami appeared relatively darker compared to the

surrounding hypomyelinated white matter (Fig. 4A). Very few patients with striatal T2W hyperintensities and none with increased striatal susceptibility were part of Cluster 2. The T2W hyperintensities in the GP were either restricted to the anterior GP (Fig. 4B) or involved the entire GP (Fig. 4C–E), rarely with adjacent striatal

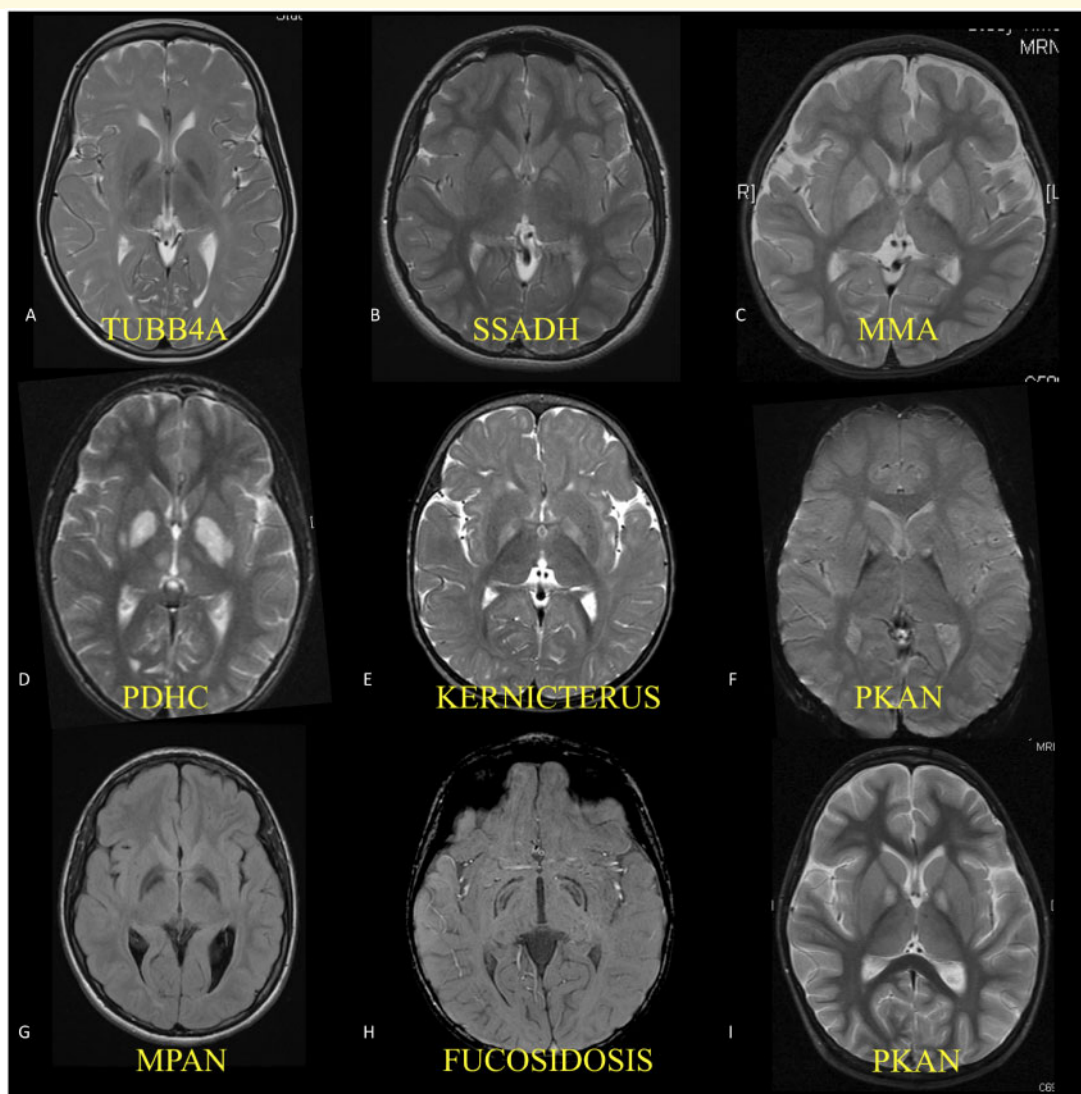


Figure 4 Cluster 2. Patterns of MRI changes seen with T2W hyperintensities or increased susceptibility in the GP in patients in Cluster 2. (A) MRI of a 6-year-old boy with a *TUBB4A* mutation showing hypomyelination of the white matter along with T2W hypointensities in bilateral globi pallidi and relatively hypointense appearing thalami due to surrounding hypomyelinated white matter; (B) MRI of a 3-year-old girl with succinic semialdehyde dehydrogenase deficiency (*SSADH*) showing T2W hyperintensities in bilateral anterior globus pallidi; (C) MRI of a 5-year-old boy with methylmalonic acidemia (*MMA*) showing T2W hyperintensities in bilateral globus pallidi; (D) MRI of a 4-year-old girl with *PDHC* showing T2W hyperintensities in bilateral globus pallidi, adjacent posterior tips of both putamina and dorsomedial nuclei of the thalamus; (E) MRI of a 1.5-year-old boy with kernicterus showing T2W hyperintensities in bilateral globi pallidi; (F) MRI of a 7-year-old boy with *PKAN* showing T2W hypointensities in bilateral globus pallidi, with persisting anterior T2W hyperintensities ('eye of the tiger'); (G) MRI image of a 6-year-old girl with *MPAN* showing T2W hypointensities in bilateral globus pallidi and sparing of bilateral internal medullary lamina; (H) Susceptibility-weighted MRI image of a 2-year-old girl with fucosidosis showing increased susceptibility in bilateral globi pallidi with sparing of the internal medullary and accessory lamina with the pallidi; (I) Earlier MRI of the same patient with *PKAN* as in 'F' at the age of 3 years showing T2W hyperintensities in bilateral anterior globus pallidi.

involvement in patients with *PDHC* (Fig. 4D). Homogenous T2W hyperintensities in the GP were noted in all 17 patients with kernicterus (Fig. 4E). Out of 39 patients with increased basal ganglia susceptibility in Cluster 2, this was noted in the GP in 37/39 patients and in the GP, SN and STN in 16/39 patients. Outside the basal ganglia nuclei, increased susceptibility was noted only in 4/85 patients in Cluster 2 (increased susceptibility

in the thalami in 2/3 patients with fucosidosis, and in the red nucleus in 2/3 patients with juvenile Huntington's disease). Most patients in Cluster 2 demonstrated either T2W hyperintensities or increased susceptibility in the GP. Three patients with pantothenate kinase-associated neurodegeneration (*PKAN*) had coexisting areas of T2W hyperintensity and increased susceptibility in the anterior portion of the medial medullary lamina of the GP

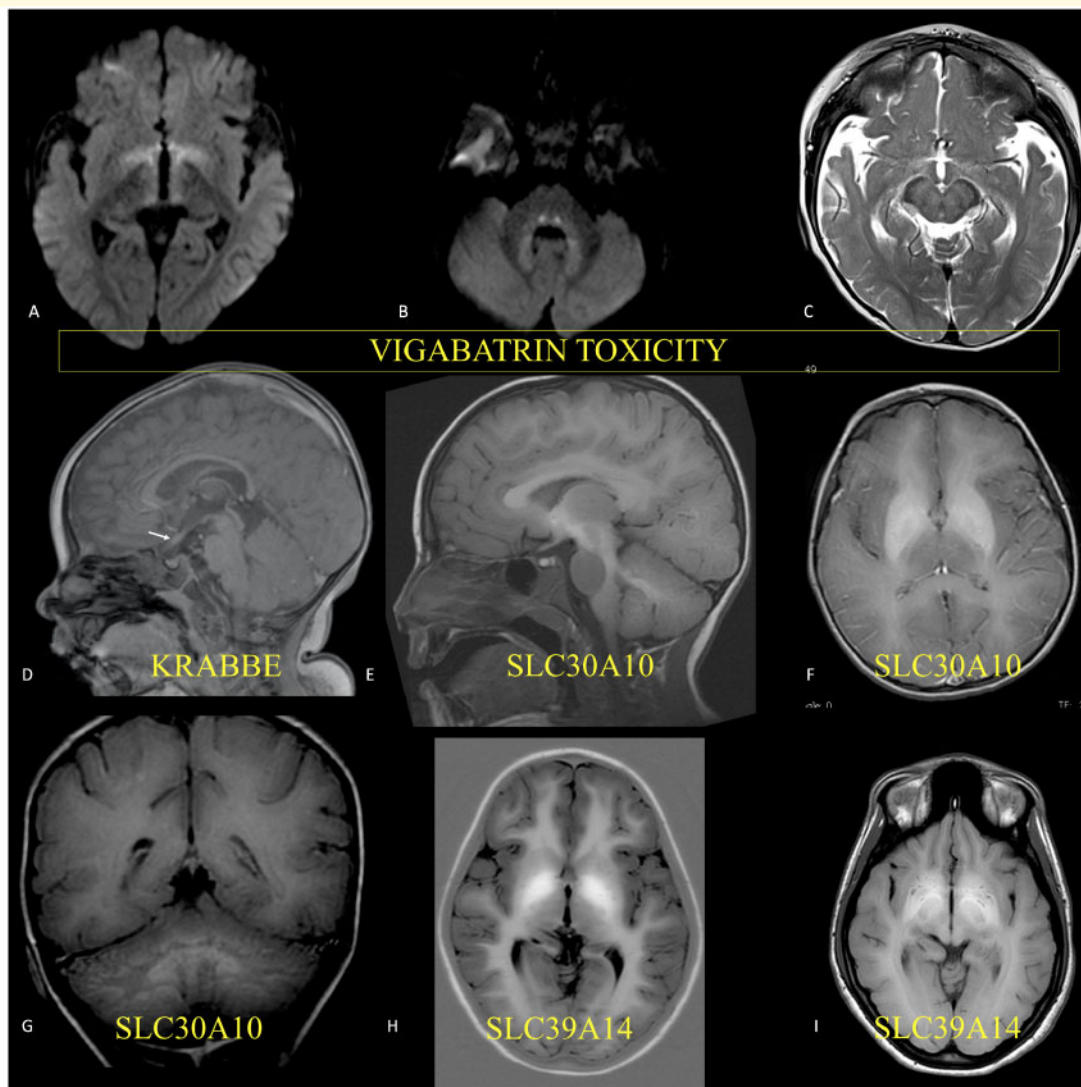


Figure 5 Clusters 3 and 4. Patterns of MRI changes in patients in Clusters 3 and 4 (**A**) Diffusion-weighted MRI of a 9-month-old boy with vigabatrin toxicity areas that were diffusion restricted—bilateral globus pallidi and ventral diencephalic regions including the hypothalamus; (**B**) Diffusion-weighted MRI of a the same patient as in 'A' with vigabatrin toxicity showing hyperintensity of the central tegmental tracts in the dorsal pons and in the dentate nuclei; (**C**) MRI of the same patient as in 'A' with vigabatrin toxicity showing T2 hyperintensities in the midbrain; (**D**) MRI of a 8-month-old girl with Krabbe disease showing expansion of the optic tract; (**E**) MRI of a 4-year-old boy with hypermanganesemia associated with *SLC30A10* showing T1W hyperintensity in a linear pattern from the GP, STN, pons to the cerebellar white matter as well as T1W hyperintensity in the anterior pituitary (**F**) MRI of the same patient as in 'E' showing diffuse T1W hyperintensities in bilateral putamen and GP as well as diffuse but less intense T1W signal change diffusely in the white matter; (**G**) MRI of the same patient as in 'E' showing T1W hyperintensity in the dentate nuclei and deep cerebellar grey matter; (**H**) MRI of an 11-year-old girl with hypermanganesemia associated with *SLC39A14* showing T1W hyperintensities in bilateral globi pallidi as well as diffuse but less intense T1W signal change diffusely in the white matter; (**I**) MRI of the same patient as in 'H' at 18 years of age showing diffuse T1W hyperintensities in bilateral caudate, putamen and GP and a rim of hyperintensity around the STN as well as diffuse T1W hyperintensity diffusely in the white matter.

resembling the 'eye of the tiger' (Fig. 4F). An identical pattern was not noted in any other diagnostic category in this cohort but some other patients demonstrated concomitant T2W hyperintensity and increased susceptibility in the GP—beta-propeller protein-associated neurodegeneration (BPAN) (1/6), gangliosidosis (1/3) and *SLC39A14* (1/6). Some patients with typical brain iron accumulation

disorders PKAN, *PLA2G6*-associated degeneration (PLAN) and BPAN only demonstrated GP T2W hyperintensities in their first scan. The medial medullary lamina in the GP was noted to be spared on T2W and susceptibility sensitive data sets in all 7/7 patients with mitochondrial membrane protein-associated neurodegeneration (MPAN) (Fig. 4G) and 1/7 patients with PLAN.

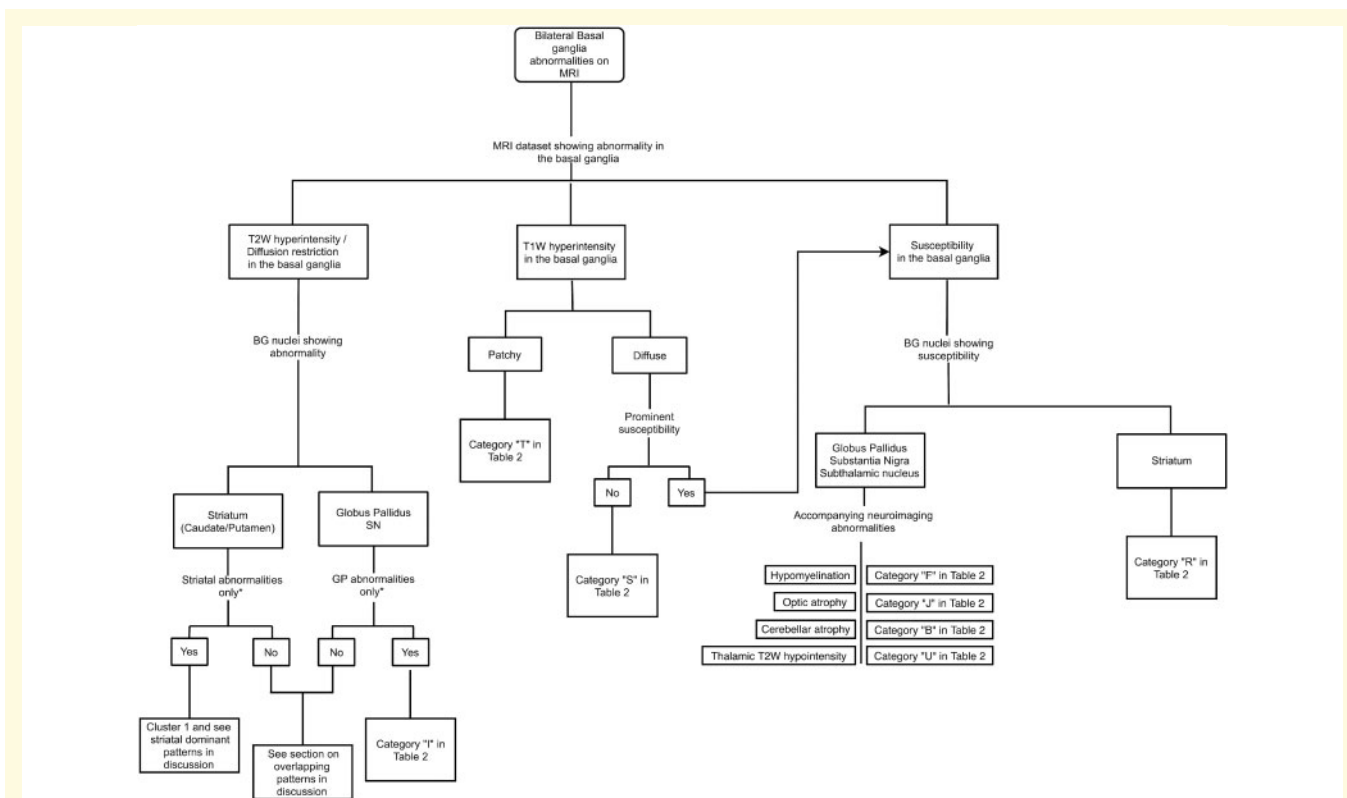


Figure 6 Branching algorithm to approach bilateral basal ganglia abnormalities on MRI. The algorithm is based on cluster analysis of MRI features from 34 diagnostic categories included in this study and review of literature of a further 59 diagnostic categories. End-points of the algorithm denoted by alphabets correspond to rows in Table 2 and to sections in discussion as noted. SN, substantia nigra. *Either striatal or GP abnormalities only amongst the basal ganglia nuclei. Other brain regions could be abnormal.

Accessory lamina in the GP appeared prominent due to sparing on T2W and susceptibility sensitive data sets in all 3/3 patients with fucosidosis (Fig. 4H).

Thirty out of 85 patients in Cluster 2 had one or more sequential MRI scans that were rated as a part of this study. There were no new MRI changes noted in patients with kernicterus. Increased susceptibility in the GP was noted on sequential scans in all those patients with PKAN (Fig. 4I), PLAN and BPAN who had demonstrated only T2W hyperintensities in the GP on their first rated MRI. All patients with MPAN (5/5) who had sequential scans demonstrated increased susceptibility in the GP, SN and STN, though the hypointensity in the GP was noted to be more prominent than the SN/STN on visual comparison. None of the sequential scans from Cluster 2 showed resolution of MRI abnormalities. Myelination was noted to be persistently immature suggesting a hypomyelinating pattern in 2/8 patients with BPAN and 5/5 patients with *TUBB4A* on their final scored sequential scans. Sequential scans were scored for all patients with *TUBB4A* noting progression of cerebellar atrophy while striatal atrophy was noted in only 2/5 patients in their final scored scans, thus not fulfilling the full radiological appearance of hypomyelination with atrophy of the basal ganglia and cerebellum. Cerebellar atrophy was noted to have progressed in all

patients with sequential scans where this had been initially noted and was noted as a new finding in one patient with Kearns Sayre syndrome on their sequential scan. Significant caudate atrophy was noted in 1/3 patients with juvenile Huntington's disease where it had been scored as normal on the first scan. Cystic changes encompassing a large part or the whole GP were noted in 3/5 patients with Kearns Sayre syndrome on sequential scans.

Cluster 3: T2W hyperintensities in the GP, brainstem and cerebellum with diffusion restriction

Eleven patients grouped together in Cluster 3 with their first MRI scans showing a combination of T2W hyperintensity in the GP and at all levels of the brainstem (Fig. 5A–C). This included all patients with vigabatrin toxicity and Krabbe disease and isolated patients with PDHC, mitochondrial translation disorder and Kearns Sayre syndrome. In addition, most MRI scans in Cluster 3 also showed T2W hyperintensities in the cerebellum and thalamus as well as accompanying diffusion restriction in the GP (Figs 2 and 5A). Prominent T2W hyperintensity and diffusion restriction was noted in the hypothalamus,

Table 1 Distribution of 201 patients across 34 included diagnostic groups fulfilling inclusion criteria

Diagnosis (arranged in alphabetical order with gene names in brackets)	N	Sex (female/male)	Mean age at first MRI scan (range) in years	Patients with follow-up MRI scans	Follow-up MRI scans Median duration of last scored scan from first scan ^a (range in years)
ADEM	11	3/8	4.7 (0.4–12.1)	6/11	0.34 (0.1–1.0)
ANE	5	3/2	4.0 (1.6–7.5)	3/5	0.9 (0.1–7.5)
ADAR-related bilateral striatal necrosis	7	3/4	2.2 (0.8–6.1)	4/7	1.4 (0.8–4.3)
BGE	10	1/9	6.3 (3.0–12.7)	7/10	0.5 (0.1–5.4)
BPAN (<i>WDR45</i>)	8	7/1	11.6 (1.3–17.0)	3/8	4 (3.9–10.6)
Cockayne syndrome (<i>ERCC8</i>)	1	0/1	7.5 ^(c)	0/1	–
Fucosidosis (<i>FUCA1</i>)	3	1/2	4.6 (2.5–7.0)	1/3	11.6 (–)
Gangliosidoses GM1 and GM2 (<i>GLB1</i> , <i>HEXA</i> , <i>GM2A</i>)	3	3/0	4.0 (1.0–10.0)	0/3	–
Glutaric aciduria type 1 (<i>GCDH</i>)	9	6/3	5.1 (5.0–11.6)	0/9	–
Hypermanganesemia with dystonia 1 (<i>SLC30A10</i>)	9	4/5	6.9 (0.1–12.0)	3/9	2.6 (0.3–4.9)
Hypermanganesemia with dystonia 2 (<i>SLC39A14</i>)	6	5/1	2.8 (1.4–5.1)	1/6	14.2 (–)
HIE (term neonates)	6	1/5	2.6 (0.8–5.5)	0/6	–
Infectious encephalitis	4	3/1	5.1 (2.2–8.7)	3/4	0.1–0.2 (0.1)
Juvenile Huntington's disease	3	2/1	10.6 (6.9–16.3)	1/3	4.5 (–)
Kearns Sayre syndrome	5	1/4	6.9 (3.2–10.5)	4/5	4.2 (2.3–6.4)
Kernicterus	17	5/12	2.6 (0.1–9.0)	5/17	1.7 (0.3–3.2)
Krabbe disease (<i>GALC</i>)	2	0/2	0.8 (0.7–0.8)	0/2	–
MEGDEL (<i>SERAC1</i>)	4	2/2	3.1 (1.2–6.9)	3/4	0.8 (0.7–4.3)
Methylmalonic acidemia (multiple genes ^b)	6	3/3	3.0 (0.5–7.6)	1/6	(–)
Mitochondrial membrane protein-associated neurodegeneration (<i>CI9orf12</i>)	8	4/4	14.1 (10.0–18.0)	5/8	1.5 (1.0–7.0)
Myelinolysis	3	1/2	8.9 (2.7–16.6)	1/3	0.5 (–)
Other mitochondrial disorders ^b	18		3.4 (0.3–11.7)		
Complex I deficiency 5		4/1		Complex I deficiency 3/5	1.7 (0.1–9.9)
Complex IV deficiency 4		2/2		Complex IV deficiency 1/4	
Complex V deficiency 8		3/5		Complex V deficiency 6/8	
Mitochondrial translation I		1/0		Mitochondrial translation 0/1	
Pantothenate kinase-associated neurodegeneration (<i>PANK2</i>)	7	4/3	7.6 (3.0–16.0)	0/7	–
<i>PLA2G6</i> -associated neurodegeneration (<i>PLA2G6</i>)	8	5/3	7.2 (1.7–14.9)	2/8	2.5 (0.2–4.7)
Propionic acidemia (<i>PCCA</i> , <i>PCCB</i>)	11	6/5	3.4 (0.1–16.0)	4/11	2.9 (2.0–13)
PDHC (multiple genes ^b)	6	2/4	6.8 (0.9–11.9)	3/6	2.2 (0.5–3.8)
Succinic semialdehyde dehydrogenase deficiency (<i>ALDH5A1</i>)	2	2/0	5.8 (1.1–10.5)	0/2	–
Thiamine responsive basal ganglia disease (<i>SLC19A3</i>)	6	3/3	5.2 (0.1–15.6)	3/6	1.7 (0.7–3.0)
<i>TUBB4A</i>	5	1/4	5.1 (1.6–10.1)	5/5	3.2 (1.0–7.9)
Vigabatrin toxicity	6	1/5	1.4 (0.7–2.8)	6/6	1.5 (0.6–1.8)
Wilson's disease (<i>ATP7B</i>)	2	0/2	15.5 (15.0–15.9)	0/2	–
TOTAL	201	92/109	5.4 (0.1–18.0)	84/201	–

MEGDEL, 3-methylglutaconic aciduria with deafness, encephalopathy and Leigh-like syndrome.

^aSingle cases—the number denotes the duration of longest follow-up for that case in years rather than the median.

^bGenotype associations in Supplementary Table 2.1.

central tegmental tracts and dentate nuclei in all patients with vigabatrin toxicity (Fig. 5B). Thickening of the optic tracts was detected in both patients with Krabbe disease (Fig. 5D) who also had white matter signal changes tracking along bilateral corticospinal tracts. One or more sequential MRI scans of 8/11 patients from Cluster 3 were available for rating. On follow-up, all MRI abnormalities had completely reverted to normal in all six patients with vigabatrin toxicity while there was persistence of abnormalities in other patients.

Cluster 4: Prominent T1W hyperintensity without accompanying T2W or DWI hyperintensity

Almost all patients with hypermanganesemia—*SLC39A14* (5/6) and *SLC30A10* (9/9) grouped together in Cluster 4 (Fig. 5–I). Patients with hypermanganesemia were distinguishable from others with T1W hyperintensity because

of diffuse, homogeneous and prominent appearance of T1W hyperintensity without accompanying T2W hyperintensity or diffusion restriction on either first or sequential scans. In this study, diffuse T1W hyperintensity in both the striatum and GP was noted in all nine patients with *SLC30A10* and 1/6 patients with *SLC39A14*. T1W hyperintensities in the GP without striatal involvement was noted in other patients with *SLC39A14*. In patients with *SLC30A10*, this was so prominent that it was not possible to discern anatomical boundaries between the caudate, putamen and GP on T1W datasets (Fig. 5F). These patients also had a typical pattern of T1W hyperintensity seen in the SN and other brain regions stretching from the basal ganglia to the cerebellum (Fig. 5E and G). Very few patients in Cluster 4 had increased susceptibility in regions that were hyperintense on T1W imaging (Fig. 2). This was in contrast to more prominent susceptibility and less prominent, patchy or partial T1W hyperintensity seen in disorders classically associated with brain iron deposition which grouped together in Cluster 2 (Fig. 4F–H) (Supplementary Fig. 3). Sequential MRI scans were available for one patient with *SLC39A14* which showed spread of T1W hyperintensity to the putamen adjoining the GP with blurring of the anatomical boundary between these nuclei (Fig. 5I).

Diagnostic algorithm and decision-making tool

On the basis of the MRI features that led to grouping of diagnostic categories in four clusters a diagnostic algorithm was designed to guide stepwise review of MRI scans with bilateral basal ganglia abnormalities. On literature review, 59 additional disease categories matching the inclusion criteria for this study were identified with reported bilateral basal ganglia MRI abnormalities. A few disorders with reported onset in adulthood such as aceruloplasminaemia and neuroferritinopathy were included as they are often considered in continuation with other genetically determined neurodegenerative disorders. In the literature review, mitochondrial disorders have been retained as in this study, categorized either based on distinct syndromes such as Kearns Sayre syndrome or MEGDEL and alternatively categorized based on biochemical findings—e.g. mitochondrial complex 1 deficiency, etc. as MRI pattern correlations in genotyped patients with mitochondrial disorders are still being described. Moreover, there is often phenotypic pleiotropy in the same genetic subgroups of mitochondrial disorders even though some genotypes can be linked to particular biochemical subgroups (Supplementary Table 2.2) (Lake *et al.*, 2016; Rahman *et al.*, 2017). Likewise, disorders with primary familial brain calcification remain grouped together. Further findings from the literature review which expand the consideration of differential diagnoses were incorporated to finalize the algorithm (Fig. 6) and the decision-making application (downloadable from

<http://www.kidsneuroscience.org.au/resources-epilepsy>) (October 2020, accessed).

Discussion

In this study, we rated 305 different MRI scans with bilateral basal ganglia lesions of children ($n=201$) with varied medical disorders ($n=34$). Four different clusters emerged based on the first MRI findings from this study cohort and all disorders segregated mainly within one of these four clusters. Moreover, in this study we use the imaging results of our cohort and those reported in literature with bilateral basal ganglia abnormalities, to derive a diagnostic algorithm and a decision-making tool. The decision-making tool incorporates a short summary of key clinical features of 91 different disorders that will further guide diagnostic evaluations in the clinical setting (also available via Supplementary Table 5).

Cluster 1 and associated conditions

The disorders that grouped together in Cluster 1 in this study had predominant striatal T2W hyperintensities with very infrequent GP abnormalities. This pattern was seen in all patients with inflammatory disorders included in this study which aligns with cases reported in the literature—both direct infectious and immune-mediated as well as auto-inflammatory syndromes. Furthermore, according to the literature, some metabolic disorders—organic acidemias and thiamine responsive basal ganglia disease associated with *SLC19A3* tend to predominantly have a striatal—Cluster 1 pattern. Likewise, this pattern has been reported in the following monogenic and neurometabolic disorders—2-Methyl-3-Hydroxybutyryl-CoA Dehydrogenase Deficiency (Cazorla *et al.*, 2007; Su *et al.*, 2017), *AFG3L2* (Eskandrani *et al.*, 2017; Tunc *et al.*, 2019), *DNAJC19* (Ucar *et al.*, 2017), giant axonal neuropathy (Hentati *et al.*, 2013), L-2-OH-glutaric aciduria (Cachia and Stine, 2013), Leber hereditary optic neuropathy (Mercuri *et al.*, 2017; Miyae *et al.*, 2019), *NUP62* (Basel-Vanagaite *et al.*, 2006), *PDE8B* (Appenzeller *et al.*, 2010; Ni *et al.*, 2019), *PDE10A* (Diggle *et al.*, 2016; Mencacci *et al.*, 2016; Esposito *et al.*, 2017; Knopp *et al.*, 2019) and *VPS13A* (Nicholl *et al.*, 2004; Lee *et al.*, 2011). While many disorders can cause homogenous T2W hyperintensity in the striatum, partial sparing of the mid-portion of the putamen, is highly suggestive of MEGDEL which has been reported in nearly all confirmed cases in one large series (Wortmann *et al.*, 2015) (Fig. 3B). In this study, partial sparing of parts of the putamen, though not as symmetric looking as seen in MEGDEL, was also noted in other mitochondrial disorders, *ADAR* and thiamine responsive basal ganglia disease (*SLC19A3*). This has been reported in literature in other mitochondrial disorders including

DNAJC19 (Ucar et al., 2017) as well as in *PDE8B* (Ni et al., 2019) and Wilson's disease.

In children with injury related to HIE at term the quite distinctive pattern of T2W hyperintensities in the motor cortex, along the corticospinal tract, including the posterior putamen and ventrolateral thalami has a high diagnostic value. Corticospinal tract abnormalities may also accompany basal ganglia MRI changes in other disorders (Table 2, category 'D'). The pattern in CP (Fig. 3E and F and Supplementary Fig. 4) which has been termed 'Rolandic type cerebral palsy' (Maller et al., 1998) may be less well recognized as it often does not show a dominant pattern of leukomalacia or cystic encephalomalacia as would be noted in antenatal HIE or HIE in preterm neonates (Rademakers et al., 1995; Huang and Castillo, 2008; Griffiths et al., 2010). Recognition of this pattern allows counselling of likely perinatal injury as the cause of CP and helps avoid further diagnostic testing. Apart from HIE, other disorders that can cause brain injury through various mechanisms can also demonstrate a striatal dominant pattern. These comprise extrapontine myelinolysis (Gocht and Colmant, 1987; Miller et al., 1988; Brown and Caruso, 1999; Bekiesinska-Figatowska et al., 2001; Ranger et al., 2012), haemolytic uraemic syndrome (Sherwood and Wagle, 1991; Jeong et al., 1994), ethylene glycol (Moore et al., 2008; Malhotra et al., 2017) and methanol poisoning (Anderson et al., 2004).

Striatal necrosis, which is a pathological diagnosis, was not scored in this study as a distinct radiological feature. Striatal atrophy, however, was observed in patients with ADAR, ADEM, ANE, glutaric aciduria type 1 (GA1), BGE, juvenile Huntington's disease, various mitochondrial disorders, MEGDEL, PDHC, *SLC19A3* and *TUBB4A*. From literature review, other disorders in which striatal atrophy on MRI has been reported include—Alexander disease, isovaleric acidemia, *MECR*, Neuroferritinopathy, *NUP62*, *PDE8B*, *PDE10A*, *PRKRA*, *UFM1*, *VAC14*, *VPS13A*, *VPS13D*, Wilson's disease, other mitochondrial disorders and as sequelae to inflammatory disorders and toxin exposure.

Cluster 2 and associated conditions

The disorders that grouped together in Cluster 2 in this study included conditions with either predominant pallidal T2W hyperintensities or those with predominant increased susceptibility in the GP. The largest diagnostic category in Cluster 2 in this study was that of patients with kernicterus. In all patients with kernicterus, there was a very consistent pattern with appearance of bilateral GP T2W hyperintensities sometimes associated with T2W hyperintensities in the SN/STN or the dentate nuclei. In some cases, the GP was atrophic, nevertheless, the pattern remained stable over time. A note of caution should be made when interpreting signal changes in the pallidum, particularly with the question of bilirubin-related neurological injury. T1W hyperintensities in the neonatal

period, similar to reported with bilirubin toxicity, can be transiently seen in normal babies in the first 3–4 weeks of life (Barkovich, 1998; Newman et al., 2002). The GP normally transitions from appearing hyperintense compared to the striatum on T2W datasets to become increasingly hypointense. T2W hyperintensities in the GP due to kernicterus may be missed as the appearance of the GP appears isointense or 'pseudonormal' compared to the neighbouring striatum during the transition phase (Shapiro, 2010; van Toorn et al., 2016) (Supplementary Fig. 5). On 1.5 T MRI, this phase is typically in the second year of life but may be evident later into early childhood if the patient is clinically delayed. Amongst genetic disorders, dominant pallidal T2W hyperintensities indicate a higher likelihood of some metabolic and mitochondrial disorders (Table 2, category 'I').

In spite of many disorders clustering to a dominant pallidal or striatal pattern of T2W hyperintensities in this study, it is evident from literature that several disorders can have MRI changes that overlap within the same or different patients namely striatal, pallidal or both pairs of nuclei showing T2W hyperintensities. In this study, concomitant pallidal and striatal T2W hyperintensities were seen in some patients with mitochondrial complex I deficiency, propionic acidemia and PDHC (Fig. 2). In the literature, this is reported in some cases with Alexander disease (van der Knaap et al., 2001; Graff-Radford et al., 2014), beta ketothiolase deficiency (Buhaş et al., 2013; O'Neill et al., 2014; Wojcik et al., 2018), Cathepsin A-related arteriopathy with strokes and leukoencephalopathy (Bugiani et al., 2016), cyanide poisoning (Rachinger et al., 2002; Beltz and Mullins, 2010), maple syrup urine disease (Gropman, 2012), metachromatic leukodystrophy (Eichler et al., 2009), sulphite oxidase and molybdenum cofactor deficiency (Tonduti et al., 2016). A similar overlap can be seen in other mitochondrial disorders, apart from those described with a dominant striatal or pallidal pattern (disorders mentioned here map to the end-point of combined striatal and pallidal T2W hyperintensities in Fig. 6).

Increased susceptibility in the pallidum and other basal ganglia nuclei may be noted in various disorders that include the deposition of paramagnetic materials such as iron deposition in the disorders of neurodegeneration with brain iron accumulation (NBIA), disorders with accumulation of copper or manganese and disorders with primary or secondary basal ganglia calcification. In addition, there are several other disorders that are designated as 'NBIA mimics' such as alpha mannosidosis, fucosidosis, gangliosidoses and mucopolidosis type IV. In our study, when the MRIs of patients with these disorders were analysed, they all grouped together in Cluster 2. *TUBB4A* and *KMT2B* should also be considered in the differential diagnosis of increased basal ganglia susceptibility (Meyer et al., 2017) in addition to several other disorders including some recent monogenic associations (Table 2)—

Table 2 Selected MRI changes and clinical features that aid narrowing down diagnostic differentials for disorders with MRI basal ganglia changes

	MRI/clinical feature	Diagnostic differential
A	Calcification accompanying brain iron deposition	BPAN CoPAN PKAN SQSTM1
B	Cerebellar atrophy with increased basal ganglia susceptibility	Aceruloplasminemia AFG3L2 Alpha mannosidosis Aspartylglucosaminuria BPAN Choline transporter-like 1 deficiency (<i>SLC44A1</i>) Congenital disorder of glycosylation, type IIa (<i>SLC39A8</i>) Cockayne syndrome FAHN Fucosidosis GM1 and GM2 Gangliosidoses GTPBP2 Kufor Rakeb syndrome Langerhans cell histiocytosis
C	Cerebellar atrophy with basal ganglia T2W hyperintensity	MPAN Mucopolipidosis type IV Neuroferritinopathy PKAN PLAN REPS1 SQSTM1 TUBB4A AFG3L2 Aspartylglucosaminuria DNAJC19 GM1 and GM2 Gangliosidoses L-2-OH-glutaric aciduria MEGDEL Mitochondrial disorders (various) PDHC Sequelae of infectious encephalitis SSADH UFM1 VPS13D Wilson's disease
D	Corticospinal tract T2W hyperintensity	3-HMG-CoA lyase deficiency CP Cerebrotendinous xanthomatosis Krabbe disease SLC19A3 VPS13D
E	Dentate T2W hyperintensities	3-HMG-COA Lyase deficiency ADEM Alexander disease Arboviral encephalitis Beta ketothiolase deficiency Canavan disease Cerebrotendinous xanthomatosis Giant axonal neuropathy Glutaric aciduria type I Kearns Sayre syndrome Kernicterus Krabbe disease L-2-OH-glutaric aciduria Langerhans cell histiocytosis Maple syrup urine disease MEGDEL

(continued)

Table 2 Continued

	MRI/clinical feature	Diagnostic differential
F	Hypomyelination with increased basal ganglia susceptibility	MMA Mitochondrial disorders (various) Neuroferritinopathy PDHC Propionic acidaemia SLC19A3 SSADH Sulphite oxidase and molybdenum cofactor deficiency Vigabatrin toxicity Wilson's disease BPAN ADAR Alpha mannosidosis Aspartylglucosaminuria Cockayne syndrome Fucosidosis GM1 and GM2 Gangliosidoses Idiopathic basal ganglia calcification Mucopolidosis type IV TUBB4A
G	Hypomyelination with basal ganglia T2W hyperintensity	3-HMG-COA Lyase deficiency Alexander disease Canavan disease Cerebral creatine deficiency syndromes GM1 and GM2 Gangliosidoses Glutaric aciduria type I Methylmalonic acidaemia Mitochondrial disorders (various—particularly Complex I deficiency) POLR3A Propionic acidaemia SSADH
H	Hypothalamus T2W hyperintensity	UFMI ADEM ANE Kearns Sayre syndrome Langerhans cell histiocytosis LHON ADEM (NMO spectrum disorder) PDHC Vigabatrin toxicity Fucosidosis
	Hypothalamus T1W hyperintensity	Manganese toxicity Liver failure (likely due to secondary manganese accumulation)
I	Mainly pallidal T2W hyperintensity without striatal abnormalities	3-HMG-COA Lyase deficiency Canavan disease Cerebrotendinous xanthomatosis Carbon monoxide poisoning Creatine deficiency syndromes—monogenic and secondary Isovaleric acidaemia Kearns Sayre syndrome Kernicterus Krabbe disease MMA PDHC SSADH
J	Optic atrophy with increased basal ganglia susceptibility	Vigabatrin toxicity AP4 deficiency FAHN Kufor Rakeb syndrome

(continued)

Table 2 Continued

	MRI/clinical feature	Diagnostic differential
K	Optic atrophy with basal ganglia T2W hyperintensity	MPAN PLAN Giant axonal neuropathy Mitochondrial disorders—LHON and others <i>MECR</i> Methanol toxicity <i>NUP62</i>
L	Optic tract/chiasm thickening	ADEM (NMO spectrum disorder) Alexander disease Krabbe disease LHON
M	Pituitary signal change/atrophy	Langerhans cell histiocytosis <i>SLC30A10</i> <i>SLC39A14</i>
N	Short stature/poor growth	Woodhouse Sakati syndrome 3-HMG-COA Lyase deficiency AP4 deficiency Choline transporter-like 1 deficiency (<i>SLC44A1</i>) Cockayne syndrome <i>KMT2B</i>
O	Retinopathy	Mitochondrial disorders 2-Methyl-3-Hydroxybutyryl-CoA Dehydrogenase Deficiency Aceruloplasminemia BPAN Kearns Sayre syndrome Methanol toxicity Mitochondrial disorders (various) Mucopolipidosis type IV PKAN <i>VAC14</i>
P	Rim of T2W hyperintensity around the putamen	ADEM ANE BGE Encephalitis—Arboviruses Gangliosidoses Metabolic acidosis Myelinolysis Propionic acidaemia <i>SLC19A3</i> Uraemia
Q	Sensorineural hearing loss	Wilson's disease 3-HMG-COA lyase deficiency Alpha mannosidosis Cockayne syndrome Kernicterus MEGDEL Metachromatic leukodystrophy <i>SCP2</i>
R	Increased striatal susceptibility	Mitochondrial disorders (various) Woodhouse Sakati syndrome Aceruloplasminemia Alpha mannosidosis Aspartylglucosaminuria Basal ganglia calcification Kufor Rakeb syndrome Multiple system atrophy Mucopolipidosis type IV Neuroferritinopathy <i>SLC30A10</i> <i>SQSTM1</i> Wilson's disease

(continued)

Table 2 Continued

	MRI/clinical feature	Diagnostic differential
S	T1W hyperintensities in the basal ganglia—Diffuse	Ephedrine toxicity Hypermanganesemia—TPN, environmental <i>SLC30A10</i> <i>SLC39A14</i> Wilson's disease (particularly with porto-systemic shunt) In association with increased basal ganglia susceptibility (less hyperintense than disorders with manganese accumulation)
T	T1W hyperintensities in the basal ganglia—Patchy	Basal ganglia calcification Carbon monoxide poisoning Cyanide poisoning <i>PDE8B</i> Sequelae of inflammatory disorders
U	T2W hypointensities in the thalamus	Alpha mannosidosis Aspartylglucosaminuria Fucosidosis Gangliosidosis Metachromatic leukodystrophy

ADEM, acute-disseminated encephalomyelitis; ANE, acute necrotizing encephalopathy; BGE, autoimmune basal ganglia encephalitis; BPAN, beta-propeller protein-associated degeneration; CoPAN, COASY protein-associated neurodegeneration; CP, cerebral palsy (due to HIE in term babies); FAHN, *FA2H*-associated neurodegeneration; LHON, Leber's hereditary optic neuropathy; MEGDEL, 3-methylglutaconic aciduria with sensori-neural deafness, encephalopathy, and Leigh-like syndrome; MMA, methyl malonic acidemia; MPAN, mitochondrial membrane protein-associated neurodegeneration; NMO, neuromyelitis optica spectrum disorder; PDHC, pyruvate dehydrogenase complex deficiency; PKAN, Panthothenate kinase-associated degeneration; PLAN, *PLA2G6*-associated neurodegeneration; SSADH, succinic semialdehyde dehydrogenase deficiency.

AP4 deficiency (Moreno-De-Luca *et al.*, 2011; Vill *et al.*, 2017; Roubertie *et al.*, 2018), *CRAT* (Drecourt *et al.*, 2018), *GTPBP2* (Jaberi *et al.*, 2016), *RAB39B* (Giannandrea *et al.*, 2010; Wilson *et al.*, 2014; Shi *et al.*, 2016), *REPS1* (Drecourt *et al.*, 2018; Levi and Tiranti, 2019), *SCP2* (Horvath *et al.*, 2015; Morarji *et al.*, 2017), *SQSTM1* (Muto *et al.*, 2018), *VPS13D* (Gauthier *et al.*, 2018; Seong *et al.*, 2018), *VAC14* (Lenk *et al.*, 2016; de Gusmao *et al.*, 2019; Lyon *et al.*, 2019), *VPS13A* (Nicholl *et al.*, 2004; Lee *et al.*, 2011), Choline transporter-like 1 deficiency (*SLC44A1*) (Fagerberg *et al.*, 2020) and Langerhans cell histiocytosis (Ertan and Huisman, 2010; Grois *et al.*, 2010; Jezierska *et al.*, 2018; de Haan *et al.*, 2019).

As noted in sequential MRI scans in our study, in patients with suspected NBIA disorders, the stage of disease progression is important in correlating MRI findings. To begin with, increased striatal susceptibility is uncommon in childhood (Table 2, category 'R'). Also, early stages of disease may not show increased susceptibility in basal ganglia nuclei in common NBIA disorders such as PLAN and PKAN (see Fig. 4F and I); furthermore, in surviving individuals, increased striatal susceptibility may develop in several classic NBIA disorders like MPAN. In a child with increased, homogenous striatal susceptibility Wilson's disease should be ruled out, and if increased striatal susceptibility is patchy or asymmetric, disorders with basal ganglia calcification should also be considered. Furthermore, iron deposition can also accompany deposition of other metals as in Wilson's disease (Dusek *et al.*, 2017, 2018). Increased susceptibility may not be seen in all patients with

neurological Wilson's disease, rather striatal T2W hyperintensities may be more obvious in childhood, as noted in this study and discussed in literature (Gupta *et al.*, 2014). In addition to clinical features, neuroimaging features that can assist in navigating differential diagnoses in the presence of increased basal ganglia susceptibility include calcification on CT scan, cerebellar atrophy, increased striatal susceptibility or atrophy, optic atrophy, hypomyelination and thalamic hypointensities (Autti *et al.*, 2007) (Table 2).

Besides primary familial brain calcification (mainly caused by *SLC20A2*, and *PDGFRB* mutations), many other disorders can lead to basal ganglia calcification (Table 2 and Supplementary Table 7). MRI patterns in some of these disorders have been previously described (Livingston *et al.*, 2013, 2014). Some patients with ADAR in particular may have pure pallidal susceptibility due to calcification on MRI rather than a Cluster 1 striatal pattern as seen in this study.

Cluster 3 and associated conditions

In this study, a distinct pattern was noted in patients with toxicity due to vigabatrin, which is a GABA transaminase inhibitor. These patients grouped together in Cluster 3 demonstrating T2W hyperintensities and diffusion restriction in the pallidum as well as the brainstem and cerebellum. Hypothalamic changes in particular were noted in all patients with vigabatrin toxicity. Only few other disorders are reported to show hypothalamic signal abnormalities accompanying basal ganglia MRI changes (Table 2, category 'H'). MRI changes are estimated to

occur in 22–32% of patients on vigabatrin (Pearl *et al.*, 2009; Wheless *et al.*, 2009), more likely to be seen in children with cryptogenic infantile spasms (Dracopoulos *et al.*, 2010). Young age and higher doses of vigabatrin have been proposed to be risk factors (Pearl *et al.*, 2009; Dracopoulos *et al.*, 2010). Other disorders in Cluster 3 included Krabbe disease and Kearns Sayre syndrome where the presence of optic tract thickening, or retinopathy, respectively, aid differential diagnosis. MRI changes in different parts of the visual pathway with basal ganglia MRI changes can help indicate some other disorders (Table 2).

Cluster 4 and associated conditions

Exceptionally prominent bilateral basal ganglia T1W hyperintensity in Cluster 4 was helpful in discerning hypermanganesemia associated with *SLC39A14* and *SLC30A10*. Even though manganese is a metal, increased susceptibility is noted in very few patients with manganese deposition. Other differentials for diffuse T1W hyperintensity in the basal ganglia include calcification, iron deposition, Wilson's disease and secondary hypermanganesemia due to occupational exposure, liver failure and ephedrone toxicity (Varlibas *et al.*, 2009) all of which have characteristic diagnostic features of their own. Toxic exposure to manganese can appear radiologically identical to the changes noted in genetically determined hypermanganesemia. In most children with *SLC39A14*, the T1W hyperintense signal seemed to remain dominantly in the GP until an older age (Fig. 5I) compared to *SLC30A10* where this diffusely involved all basal ganglia nuclei even at an early age, always including the GP. In contrast, disorders with basal ganglia calcification may sometimes show striatal T1W hyperintensities without involving the GP and *vice versa*. Patchy T1W hyperintensities may often be noted with resolving haemorrhagic change or dystrophic calcification after the acute phase of several disorders including inflammatory disorders, episodes of decompensation in metabolic, including mitochondrial disorders or toxin exposure as well as in cases of bilateral basal ganglia neoplasia which we have not reviewed here. Although quantification of signal change is not routinely possible in clinical practice, the T1W hyperintensity noted with manganese deposition is much brighter and diffuse than seen in other disorders.

Importance of basal ganglia MRI pattern recognition and study limitations

The ascertainment of paediatric neurological conditions with basal ganglia involvement is best accomplished first with defining the clinical phenotype in detail. Subsequently, the recognition of characteristic MRI patterns in the basal ganglia can help to consider either a

single entity or a short list of differentials with the aim of rationalizing clinical testing. A pattern that may be typical of monophasic ADEM, BGE, CP or kernicterus for example, should subsequently obviate the need to keep repeating MRI scans or pursue other unnecessary investigations. In the correct clinical context, if the imaging pattern fits a treatable disorder such as BGE, ADEM or, *SLC19A3* empiric treatment may be instituted while awaiting other results. In the same vein, some patterns, such as the 'eye of the tiger' or the 'face of the giant panda' tend to become associated with certain diseases as pathognomonic associations. However, the absence of such patterns may indicate an early stage of the disease and should not lead to exclusion of these differentials. Our retrospective study design did enable cross-sectional comparisons between diseases but did not permit accurate longitudinal assessment of resolution or progression of imaging features.

Sometimes, the finding of changes in parts of the brain that are not classically involved in a particular disease, may be described as an 'expansion of the phenotype'. These may at times, be due to comorbid conditions or complications, for example, immature myelination in one patient with kernicterus in this study was likely due to extreme prematurity. Likewise, metabolic disturbances like hypoglycaemia in disorders like 3-HMG-CoA lyase deficiency, 2-Methyl-3-Hydroxybutyryl-CoA dehydrogenase deficiency may lead to occipital changes typical of low glucose levels.

Our study was performed using a retrospective cohort where MRI scans were done as part of the standard clinical evaluation in children with different neurological disorders; therefore, there was an inherent variability in the MRI protocols, having used different machines and image acquisition timing. The major inclusion criteria in this study and for the cases selected from the literature was the obligatory presence of bilateral basal ganglia MRI abnormalities. The differentials and approach discussed here only become relevant in patients with those disorders when there is bilateral basal ganglia abnormality to start with. Some disorders included in this study may actually have a more typical and common MRI appearance that may not involve the basal ganglia. This study cohort was heterogeneous with different patient numbers for included diagnostic categories, and some of the groups had very small numbers of patients. Therefore, MRI features that are not always seen in a diagnostic category may have been missed. Also, MRI changes seen transiently may not have been obvious in scans in this study that were done later in the disease course, for example diffusion restriction is only present in the newborn period for babies with HIE.

The primary raters were not blinded to the diagnostic categories leaving a major potential for bias to over-reporting well-known imaging features while under-reporting unusual, unrecognized or novel MRI features. In order to balance against these caveats, a subset of

patients was rated by three independent radiologists who were blinded to each other's ratings and we leveraged by performing a literature review and incorporating other findings into Table 2 and the subsequent decision-making tool. Lastly, this cohort and study were restricted to childhood-onset disorders. Although there may be similarities and overlap with adult-onset disorders, it is likely there would be disease-related and radiological phenotypic differences in adult-onset disorders—future studies could develop an adult-onset cohort for study.

Conclusion

In children with neurological symptoms and MRI abnormalities affecting the basal ganglia, clustering of neuroimaging patterns as described in this study can complement clinical information to aid differential diagnosis and guide diagnostic testing. This pattern recognition approach to basal ganglia disorders may help identify currently unrecognized patient subgroups that could increase the yield of genetic testing. We propose the use of the neuroimaging clusters and diagnostic algorithm described here in children with bilateral basal ganglia MRI lesions. Prospective evaluation of this pattern approach and of the prototypic electronic tool in larger cohorts, including machine learning approaches may optimize their overall diagnostic accuracy and validity.

Supplementary material

Supplementary material is available at *Brain Communications* online.

Acknowledgements

The authors acknowledge all contributing clinicians and patients as well as technical staff in the department of Radiology at the Children's hospital at Westmead, Great Ormond Street Hospital and Oregon Health and Science University, Portland. The authors also acknowledge other members of Manju Kurian's group at UCL—Dr Amy McTague, Dr Adeline Ngoh and Dr Esther Meyer, who assisted with patient identification and project methodology. S.S.M. and R.C.D. acknowledge support from Cerebral palsy alliance, Allambie Heights, Sydney. The authors acknowledge assistance from Amanda Laing, Himanshu Joshi and Leigh Waddell from Kids Neuroscience, Westmead, Australia to upload and host the electronic decision-making tool.

Funding

S.S.M. received funding via a competitive scholarship from the Winston Churchill Memorial trust of Australia to enable

travel for this study and held postgraduate research scholarships from the National Health and Medical Research Council, Australia and the Petre foundation at the time of this study.

Competing interests

None of the authors have any competing interests to declare. All research at Great Ormond Street Hospital NHS Foundation Trust and UCL Great Ormond Street Institute of Child Health is made possible by the National institute for health research, (NIHR) Great Ormond Street Hospital Biomedical Research Centre. The views expressed are those of the author(s) and not necessarily those of the NHS, the NIHR or the Department of Health.

References

- Anderson JC, Costantino MM, Stratford T. Basal ganglia: anatomy, pathology, and imaging characteristics. *Curr Probl Diagn Radiol* 2004; 33: 28–41.
- Appenzeller S, Schirmacher A, Halfter H, Baumer S, Pendziwiat M, Timmerman V, et al. Autosomal-dominant striatal degeneration is caused by a mutation in the phosphodiesterase 8B gene. *Am J Hum Genet* 2010; 86: 83–7.
- Autti T, Joensuu R, Aberg L. Decreased T2 signal in the thalami may be a sign of lysosomal storage disease. *Neuroradiology* 2007; 49: 571–8.
- Barkovich AJ. MR of the normal neonatal brain: assessment of deep structures. *AJNR Am J Neuroradiol* 1998; 19: 1397–403.
- Basel-Vanagaite L, Muncher L, Straussberg R, Pasmanik-Chor M, Yahav M, Rainshtein L, et al. Mutated nup62 causes autosomal recessive infantile bilateral striatal necrosis. *Ann Neurol* 2006; 60: 214–22.
- Bekiesińska-Figatowska M, Bulski T, Rózycka I, Furmanek M, Walecki J. MR imaging of seven presumed cases of central pontine and extrapontine myelinolysis. *Acta Neurobiol Exp (Wars)* 2001; 61: 141–4.
- Bekiesińska-Figatowska M, Mierzewska H, Jurkiewicz E. Basal ganglia lesions in children and adults. *Eur J Radiol* 2013; 82: 837–49.
- Beltz EE, Mullins ME. Radiological reasoning: hyperintensity of the basal ganglia and cortex on FLAIR and diffusion-weighted imaging. *AJR Am J Roentgenol* 2010; 195 (Suppl):S9–S11.
- Brown WD, Caruso JM. Extrapontine myelinolysis with involvement of the hippocampus in three children with severe hyponatremia. *J Child Neurol* 1999; 14: 428–33.
- Bugiani M, Kevelam SH, Bakels HS, Waisfisz Q, Ceuterick-de Groote C, Niessen HWM, et al. Cathepsin A-related arteriopathy with strokes and leukoencephalopathy (CARASAL). *Neurology* 2016; 87: 1777–86.
- Buhaş D, Bernard G, Fukao T, Décarie J-C, Chouinard S, Mitchell GA. A treatable new cause of chorea: beta-ketothiolase deficiency. *Mov Disord* 2013; 28: 1054–6.
- Cachia D, Stine C. Child neurology: cognitive delay in a 7-year-old girl. *Neurology* 2013; 81: e148–50.
- Cazorla MR, Verdu A, Perez-Cerda C, Ribes A. Neuroimage findings in 2-methyl-3-hydroxybutyryl-CoA dehydrogenase deficiency. *Pediatr Neurol* 2007; 36: 264–7.
- Charrad M, Ghazzali N, Boiteau V, Niknafs A, Charrad MM. Package 'nbclust'. *J Stat Software* 2014; 61: 1–36.
- Diggle CP, Sukoff Rizzo SJ, Popielek M, Hinttala R, Schülke J-P, Kurian MA, et al. Biallelic mutations in PDE10A lead to loss of

- striatal PDE10A and a hyperkinetic movement disorder with onset in infancy. *Am J Hum Genet* 2016; 98: 735–43.
- Dracopoulos A, Widjaja E, Raybaud C, Westall CA, Snead OC 3rd. Vigabatrin-associated reversible MRI signal changes in patients with infantile spasms. *Epilepsia* 2010; 51: 1297–304.
- Drecourt A, Babdor J, Dussiot M, Petit F, Goudin N, Garfa-Traoré M, et al. Impaired transferrin receptor palmitoylation and recycling in neurodegeneration with brain iron accumulation. *Am J Hum Genet* 2018; 102: 266–77.
- Dusek P, Bahn E, Litwin T, Jablonka-Salach K, Łuciuk A, Huelnhagen T, et al. Brain iron accumulation in Wilson disease: a post mortem 7 Tesla MRI—histopathological study. *Neuropathol Appl Neurobiol* 2017; 43: 514–32.
- Dusek P, Skoloudik D, Maskova J, Huelnhagen T, Bruha R, Zahorakova D, et al. Brain iron accumulation in Wilson's disease: a longitudinal imaging case study during anticopper treatment using 7.0T MRI and transcranial sonography. *J Magn Reson Imaging* 2018; 47: 282–5.
- Eichler F, Grodd W, Grant E, Sessa M, Biffi A, Bley A, et al. Metachromatic leukodystrophy: a scoring system for brain MR imaging observations. *AJNR Am J Neuroradiol* 2009; 30: 1893–7.
- Ertan G, Huisman T. Susceptibility-weighted imaging in neurodegeneration in Langerhans cell histiocytosis. *J Pediatr* 2010; 156: 1032.
- Eskandrani A, AlHashem A, Ali ES, AlShahwan S, Tlili K, Hundallah K, et al. Recessive AFG3L2 mutation causes progressive microcephaly, early onset seizures, spasticity, and basal ganglia involvement. *Pediatr Neurol* 2017; 71: 24–8.
- Esposito S, Carecchio M, Tonduti D, Saletti V, Panteghini C, Chiapparini L, et al. A PDE10A de novo mutation causes childhood-onset chorea with diurnal fluctuations. *Mov Disord* 2017; 32: 1646–7.
- Fagerberg CR, Taylor A, Distelmaier F, Schröder HD, Kibæk M, Wiczorek D, et al. Choline transporter-like 1 deficiency causes a new type of childhood-onset neurodegeneration. *Brain* 2020; 143: 94–111.
- Fahn S. Biochemistry of the basal ganglia. *Adv Neurol* 1976; 14: 59–89.
- Finelli PF, DiMario FJ Jr. Diagnostic approach in patients with symmetric imaging lesions of the deep gray nuclei. *Neurologist* 2003; 9: 250–61.
- Fleiss JL. Measuring nominal scale agreement among many raters. *Psychol Bull* 1971; 76: 378–82.
- Gauthier J, Meijer IA, Lessel D, Mencacci NE, Krainc D, Hempel M, et al. Recessive mutations in VPS13D cause childhood onset movement disorders. *Ann Neurol* 2018; 83: 1089–95.
- Giannandrea M, Bianchi V, Mignogna ML, Sirri A, Carrabino S, D'Elia E, et al. Mutations in the small GTPase gene RAB39B are responsible for X-linked mental retardation associated with autism, epilepsy, and macrocephaly. *Am J Hum Genet* 2010; 86: 185–95.
- Gocht A, Colmant HJ. Central pontine and extrapontine myelinolysis: a report of 58 cases. *Clin Neuropathol* 1987; 6: 262–70.
- Graff-Radford J, Schwartz K, Gavrillova RH, Lachance DH, Kumar N. Neuroimaging and clinical features in type II (late-onset) Alexander disease. *Neurology* 2014; 82: 49–56.
- Griffiths PD, Radon MR, Crossman AR, Zurakowski D, Connolly DJ. Anatomic localization of dyskinesia in children with “profound” perinatal hypoxic-ischemic injury. *AJNR Am J Neuroradiol* 2010; 31: 436–41.
- Grois N, Fahrner B, Arceci RJ, Henter JI, McClain K, Lassmann H, et al. Central nervous system disease in Langerhans cell histiocytosis. *J Pediatr* 2010; 156: 873–81.e1.
- Gropman AL. Patterns of brain injury in inborn errors of metabolism. *Semin Pediatr Neurol* 2012; 19: 203–10.
- Gupta A, Chakravarthi S, Goyal MK. ‘Face of giant panda’: a rare imaging sign in Wilson's disease. *QJM* 2014; 107: 579.
- Gusmao CM, Stone S, Waugh JL, Yang E, Lenk GM, Rodan LH. VAC14 gene-related parkinsonism-dystonia with response to deep brain stimulation. *Mov Disord Clin Pract* 2019; 6: 494–7.
- Haan S, Velden WJFM, Meijer FJA. Striatal involvement in neurodegenerative langerhans cell histiocytosis. *Mov Disord Clin Pract* 2019; 6: 719–21.
- Hegde AN, Mohan S, Lath N, Lim CC. Differential diagnosis for bilateral abnormalities of the basal ganglia and thalamus. *Radiographics* 2011; 31: 5–30.
- Hentati F, Hentati E, Amouri R. Giant axonal neuropathy. *Handb Clin Neurol* 2013; 115: 933–8.
- Ho VB, Fitz CR, Chuang SH, Geyer CA. Bilateral basal ganglia lesions: pediatric differential considerations. *Radiographics* 1993; 13: 269–92.
- Horvath R, Lewis-Smith D, Douroudis K, Duff J, Keogh M, Pyle A, et al. SCP2 mutations and neurodegeneration with brain iron accumulation. *Neurology* 2015; 85: 1909–11.
- Huang BY, Castillo M. Hypoxic-ischemic brain injury: imaging findings from birth to adulthood. *Radiographics* 2008; 28: 417–39; quiz 617.
- Jaberi E, Rohani M, Shahidi GA, Nafissi S, Arefian E, Soleimani M, et al. Identification of mutation in GTPBP2 in patients of a family with neurodegeneration accompanied by iron deposition in the brain. *Neurobiol Aging* 2016; 38: e11–8.
- Jeong YK, Kim IO, Kim WS, Hwang YS, Choi Y, Yeon KM. Hemolytic uremic syndrome: MR findings of CNS complications. *Pediatr Radiol* 1994; 24: 585–6.
- Jeziarska M, Stefanowicz J, Romanowicz G, Kosiak W, Lange M. Langerhans cell histiocytosis in children—a disease with many faces. Recent advances in pathogenesis, diagnostic examinations and treatment. *Postepy Dermatol Alergol* 2018; 35: 6–17.
- Knopp C, Hausler M, Muller B, Damen R, Stoppe A, Mull M, et al. PDE10A mutation in two sisters with a hyperkinetic movement disorder—response to levodopa. *Parkinsonism Relat Disord* 2019; 63: 240–2.
- Krageloh-Mann I, Helber A, Mader I, Staudt M, Wolff M, Groenendaal F, et al. Bilateral lesions of thalamus and basal ganglia: origin and outcome. *Dev Med Child Neurol* 2002; 44: 477–84.
- Lake NJ, Compton AG, Rahman S, Thorburn DR. Leigh syndrome: one disorder, more than 75 monogenic causes. *Ann Neurol* 2016; 79: 190–203.
- Lee JH, Lee SM, Baik SK. Demonstration of striatopallidal iron deposition in chorea-acanthocytosis by susceptibility-weighted imaging. *J Neurol* 2011; 258: 321–2.
- Lenk GM, Szymanska K, Debska-Vielhaber G, Rydzanicz M, Walczak A, Bekiesinska-Figatowska M, et al. Biallelic mutations of VAC14 in pediatric-onset neurological disease. *Am J Hum Genet* 2016; 99: 188–94.
- Levi S, Tiranti V. Neurodegeneration with brain iron accumulation disorders: valuable models aimed at understanding the pathogenesis of iron deposition. *Pharmaceuticals* 2019; 12: 27.
- Lim C. Magnetic resonance imaging findings in bilateral basal ganglia lesions. *Ann Acad Med Singap* 2009; 38: 795–8.
- Livingston JH, Stivaros S, van der Knaap MS, Crow YJ. Recognizable phenotypes associated with intracranial calcification. *Dev Med Child Neurol* 2013; 55: 46–57.
- Livingston JH, Stivaros S, Warren D, Crow YJ. Intracranial calcification in childhood: a review of aetiologies and recognizable phenotypes. *Dev Med Child Neurol* 2014; 56: 612–26.
- Lyon GJ, Marchi E, Ekstein J, Meiner V, Hirsch Y, Scher S, et al. VAC14 syndrome in two siblings with retinitis pigmentosa and neurodegeneration with brain iron accumulation. *Cold Spring Harb Mol Case Stud* 2019; 5: a003715.
- Malhotra A, Mongelluzzo G, Wu X, Durand D, Kalra VB, LeSar B, et al. Ethylene glycol toxicity: MRI brain findings. *Clin Neurol* 2017; 27: 109–13.
- Maller AI, Hankins LL, Yeakley JW, Butler IJ. Rolandic type cerebral palsy in children as a pattern of hypoxic-ischemic injury in the full-term neonate. *J Child Neurol* 1998; 13: 313–21.
- Mencacci NE, Kamsteeg E-J, Nakashima K, R'Bibo L, Lynch DS, Balint B, et al. De novo mutations in PDE10A cause childhood-onset

- chorea with bilateral striatal lesions. *Am J Hum Genet* 2016; 98: 763–71.
- Mercuri MA, White H, Oliveira C. Vision loss and symmetric basal ganglia lesions in leber hereditary optic neuropathy. *J Neuroophthalmol* 2017; 37: 411–3.
- Meyer E, Carss KJ, Rankin J, Nichols JM, Grozeva D, Joseph AP, et al.; UK10K Consortium. Mutations in the histone methyltransferase gene *KMT2B* cause complex early-onset dystonia. *Nat Genet* 2017; 49: 223–37.
- Miller GM, Baker HL Jr, Okazaki H, Whisnant JP. Central pontine myelinolysis and its imitators: MR findings. *Radiology* 1988; 168: 795–802.
- Miyae N, Yamanishi Y, Tada S, Ando R, Yabe H, Nagai M, et al. Repetitive brainstem lesions in mitochondrial DNA 11778G>A mutation of Leber hereditary optic neuropathy. *eNeurologicalSci* 2019; 14: 74–6.
- Moore MM, Kanekar SG, Dhamija R. Ethylene glycol toxicity: chemistry, pathogenesis, and imaging. *Radiol Case Rep* 2008; 3: 122.
- Morarji J, Gillespie R, Sergouniotis PI, Horvath R, Black GCM. An unusual retinal phenotype associated with a mutation in sterol carrier protein *SCP2*. *JAMA Ophthalmol* 2017; 135: 167–9.
- Moreno-De-Luca A, Helmers SL, Mao H, Burns TG, Melton AM, Schmidt KR, et al. Adaptor protein complex-4 (*AP-4*) deficiency causes a novel autosomal recessive cerebral palsy syndrome with microcephaly and intellectual disability. *J Med Genet* 2011; 48: 141–4.
- Muto V, Flex E, Kupchinsky Z, Primiano G, Galehdari H, Dehghani M, et al. Biallelic *SQSTM1* mutations in early-onset, variably progressive neurodegeneration. *Neurology* 2018; 91: e319–30.
- Newman TB, Maisels MJ, Zimmerman RA, Harris MC. Magnetic resonance imaging and kernicterus. *Pediatrics* 2002; 109: 555–555.
- Ni J, Yi X, Liu Z, Sun W, Yuan Y, Yang J, et al. Clinical findings of autosomal-dominant striatal degeneration and *PDE8B* mutation screening in parkinsonism and related disorders. *Parkinsonism Relat Disord* 2019; 69: 94–8.
- Nicholl DJ, Sutton I, Dotti MT, Supple SG, Danek A, Lawden M. White matter abnormalities on MRI in neuroacanthocytosis. *J Neurol Neurosurg Psychiatry* 2004; 75: 1200–1.
- O'Neill ML, Kuo F, Saigal G. MRI of pallidal involvement in Beta-ketothiolase deficiency. *J Neuroimaging* 2014; 24: 414–7.
- Pearl PL, Vezina LG, Saneto RP, McCarter R, Molloy-Wells E, Heffron A, et al. Cerebral MRI abnormalities associated with vigabatrin therapy. *Epilepsia* 2009; 50: 184–94.
- Pillai SC, Hacohen Y, Tantsis E, Prelog K, Merheb V, Kesson A, et al. Infectious and autoantibody-associated encephalitis: clinical features and long-term outcome. *Pediatrics* 2015; 135: e974.
- Quattrocchi CC, Longo D, Delfino LN, Errante Y, Aiello C, Fariello G, et al. MR differential diagnosis of acute deep grey matter pathology in paediatric patients. *Pediatr Radiol* 2013; 43: 743–61.
- R Core Team. R: a language and environment for statistical computing, version 3.0. 2. Vienna, Austria: R Foundation for Statistical Computing; 2019.
- Rachinger J, Fellner FA, Stieglbauer K, Trenkler J. MR changes after acute cyanide intoxication. *AJNR Am J Neuroradiol* 2002; 23: 1398–401.
- Rademakers RP, van der Knaap MS, Verbeeten B Jr, Barth PG, Valk J. Central cortico-subcortical involvement: a distinct pattern of brain damage caused by perinatal and postnatal asphyxia in term infants. *J Comput Assist Tomogr* 1995; 19: 256–63.
- Rahman J, Noronha A, Thiele I, Rahman S. Leigh map: a novel computational diagnostic resource for mitochondrial disease. *Ann Neurol* 2017; 81: 9–16.
- Ranger AM, Chaudhary N, Avery M, Fraser D. Central pontine and extrapontine myelinolysis in children: a review of 76 patients. *J Child Neurol* 2012; 27: 1027–37.
- Roubertie A, Hieu N, Roux CJ, Leboucq N, Manes G, Charif M, et al. *AP4* deficiency: a novel form of neurodegeneration with brain iron accumulation? *Neurol Genet* 2018; 4: e217.
- Seong E, Insolera R, Dulovic M, Kamsteeg EJ, Trinh J, Bruggemann N, et al. Mutations in *VPS13D* lead to a new recessive ataxia with spasticity and mitochondrial defects. *Ann Neurol* 2018; 83: 1075–88.
- Shapiro SM. Chronic bilirubin encephalopathy: diagnosis and outcome. *Semin Fetal Neonatal Med* 2010; 15: 157–63.
- Sherwood JW, Wagle WA. Hemolytic uremic syndrome: MR findings of CNS complications. *AJNR Am J Neuroradiol* 1991; 12: 703–4.
- Shi CH, Zhang SY, Yang ZH, Yang J, Shang DD, Mao CY, et al. A novel *RAB39B* gene mutation in X-linked juvenile parkinsonism with basal ganglia calcification. *Mov Disord* 2016; 31: 1905–9.
- Steenweg ME, Vanderver A, Blaser S, Bizzi A, de Koning TJ, Mancini GM, et al. Magnetic resonance imaging pattern recognition in hypomyelinating disorders. *Brain* 2010; 133: 2971–82.
- Su L, Li X, Lin R, Sheng H, Feng Z, Liu L. Clinical and molecular analysis of 6 Chinese patients with isoleucine metabolism defects: identification of 3 novel mutations in the *HSD17B10* and *ACAT1* gene. *Metab Brain Dis* 2017; 32: 2063–71.
- Tonduti D, Chiapparini L, Moroni I, Ardissona A, Zorzi G, Zibordi F, et al. Neurological disorders associated with striatal lesions: classification and diagnostic approach. *Curr Neurol Neurosci Rep* 2016; 16: 54.
- Tunc S, Dulovic-Mahlow M, Baumann H, Baaske MK, Jahn M, Junker J, et al. Spinocerebellar ataxia type 28-phenotypic and molecular characterization of a family with heterozygous and compound-heterozygous mutations in *AFG3L2*. *Cerebellum* 2019; 18: 817–22.
- Ucar SK, Mayr JA, Feichtinger RG, Canda E, Coker M, Wortmann SB. Previously unreported biallelic mutation in *DNAJC19*: are sensorineural hearing loss and basal ganglia lesions additional features of dilated cardiomyopathy and ataxia (DCMA) syndrome? *JIMD Rep* 2017; 35: 39–45.
- van der Knaap MS, Breiter SN, Naidu S, Hart AA, Valk J. Defining and categorizing leukoencephalopathies of unknown origin: MR imaging approach. *Radiology* 1999; 213: 121–33.
- van der Knaap MS, Naidu S, Breiter SN, Blaser S, Stroink H, Springer S, et al. Alexander disease: diagnosis with MR imaging. *AJNR Am J Neuroradiol* 2001; 22: 541–52.
- van der Knaap MS, Valk J, de Neeling N, Nauta JJ. Pattern recognition in magnetic resonance imaging of white matter disorders in children and young adults. *Neuroradiology* 1991; 33: 478–93.
- van Toorn R, Brink P, Smith J, Ackermann C, Solomons R. Bilirubin-induced neurological dysfunction: a clinico-radiological-neurophysiological correlation in 30 consecutive children. *J Child Neurol* 2016; 31: 1579–83.
- Varlibas F, Delipoyraz I, Yuksel G, Filiz G, Tireli H, Gecim NO. Neurotoxicity following chronic intravenous use of “Russian cocktail”. *Clin Toxicol (Phila)* 2009; 47: 157–60.
- Vill K, Muller-Felber W, Alhaddad B, Strom TM, Teusch V, Weigand H, et al. A homozygous splice variant in *AP4S1* mimicking neurodegeneration with brain iron accumulation. *Mov Disord* 2017; 32: 797–9.
- Wheless JW, Carmant L, Bebin M, Conry JA, Chiron C, Elterman RD, et al. Magnetic resonance imaging abnormalities associated with vigabatrin in patients with epilepsy. *Epilepsia* 2009; 50: 195–205.
- Wilson GR, Sim JC, McLean C, Giannandrea M, Galea CA, Riseley JR, et al. Mutations in *RAB39B* cause X-linked intellectual disability and early-onset Parkinson disease with alpha-synuclein pathology. *Am J Hum Genet* 2014; 95: 729–35.

- Wojcik MH, Wierenga KJ, Rodan LH, Sahai I, Ferdinandusse S, Genetti CA, et al. Beta-ketothiolase deficiency presenting with metabolic stroke after a normal newborn screen in two individuals. *JIMD Rep* 2018; 39: 45–54.
- Wortmann SB, van Hasselt PM, Baric I, Burlina A, Darin N, Horster F, et al. Eyes on MEGDEL: distinctive basal ganglia involvement in dystonia deafness syndrome. *Neuropediatrics* 2015; 46: 98–103.
- Zuccoli G, Yannes MP, Nardone R, Bailey A, Goldstein A. Bilateral symmetrical basal ganglia and thalamic lesions in children: an update (2015). *Neuroradiology* 2015; 57: 973–89.

Appendix

Basal ganglia MRI Study Group: Manoj P. Menezes, Sachin Gupta, Christopher Troedson, Sekhar Pillai, Esther Tantsis, Deepak Gill, Carolyn Ellaway, Simone Ardern Holmes, Jayne Antony, Kshitij Mankad, Lucinda Carr, Prab Prabhakar, Pinki Munot, Sanjay Bhate, Paul Gissen, Peter Clayton, Karin Tuschl, Louise Simmons, Yanick Crow and Troy Dalkeith.